
The polygon model for 2+1D gravity: the constraint algebra and problems of quantization

Jaap Eldering

7th June 2006

Masters thesis
supervised by Prof. Renate Loll
Institute for Theoretical Physics
Utrecht University



Abstract

In this thesis we consider 't Hooft's polygon model for 2+1D gravity. We first recall the ADM formalism to write general relativity in Hamiltonian form. With this background in mind, we give a detailed review of the polygon model and its explicit evolution description in the classical context.

Then we review some remarks in the literature about quantization of this model and the discreteness of space-time. We discuss the problems associated with this in the context of canonical quantization for some explicit quantization schemes: the triangle inequalities conflict with the Stone–Von Neumann uniqueness theorem when we use the canonical variables. Also, the implementation of transitions, the constraints and their algebra poses significant problems. We conclude that no rigorous conclusions about the spectrum of space-time can be drawn without an explicit quantization scheme.

Furthermore, we consider the Poisson structure of the constraints, which are important when we try to quantize the model. We improve known results and show that the full Poisson structure can be calculated explicitly and that it closes on shell. An attempt is made to interpret the gauge orbits generated by the constraints.

Contents

1	Introduction	3
1.1	Gravity: general relativity	3
1.2	Quantization	4
1.3	The polygon model	4
2	Notation and conventions	5
3	Representing gravity	9
3.1	Foliation of space-time	9
3.2	Hamiltonian formulation	11
3.3	Reduction of phase space	12
4	The polygon model	14
4.1	Tessellation of the spatial surface	15
4.2	Vertex relations	17
4.3	Constraints	18
4.4	Dynamics	19
4.5	Transitions	21
4.6	Constrained dynamics	23
4.7	Simulation	26
5	Quantization	27
5.1	General procedure	28
5.2	Constraints in quantization	29

5.3	Quantization of the polygon model	31
5.4	Conclusions	35
6	The constraint algebra	36
6.1	Useful formulas	37
6.2	Calculation of the algebra	40
6.3	Generalizations	47
6.4	Summary	54
6.5	Interpretation	55
7	Conclusions	57
A	The dual graph	59
A.1	The dual of a planar graph	59
A.2	Hyperbolic space	61
A.3	Embedding the dual graph in \mathbb{H}^2	62
	Bibliography	66

1 Introduction

In this thesis we will study a particular model for (Einstein) gravity: the 't Hooft polygon model for gravity in $2+1$ -dimensions. We will specifically be concerned with the question of whether this model can be quantized and we calculate the complete Poisson structure of the constraints.

The $2+1$ here stands for 2 spatial dimensions and 1 time dimension. This is one dimension lower than the $3+1$ -dimensions we (seem to) live in. That turns out to make the whole problem a lot simpler than trying to tackle the full problem of four-dimensional quantum gravity, which people are trying to solve for decades already. It is hoped then, that by studying and hopefully solving three-dimensional (and in general lower dimensional) quantum gravity, we can learn something about how to solve four-dimensional quantum gravity.

1.1 Gravity: general relativity

When we say ‘gravity’ we mean the classical theory of gravity as formulated by Albert Einstein, which is known as ‘general relativity’. It has as a starting point that (locally) the effect of a gravitational field and acceleration are the same.

This has as consequences that space and time together (often referred to as space-time) can be curved: the concept of a straight line is not entirely lost, but becomes somewhat more subtle. For example in a curved space it can be possible to always travel in a straight line and come back to where you started, or that two straight lines intersect each other at more than one point.

The mathematical description of this theory is much more complicated than that of the classical, Newtonian theory of gravity and finding solutions is much more difficult, already in the classical (non-quantum) theory.

On the other hand, general relativity describes some interesting phenomena. Some of these are already well confirmed by measurements, like the bending of light rays by large masses (e.g. the sun) and the slowing of time in gravitational wells. Other phenomena are predicted but not yet detected, like black holes and gravitational waves.

1.2 Quantization

At the start of the 20th century, physical phenomena were discovered which could not be described by the classical physical theories. Examples are the photo-electric effect and the observed structure of atoms.

A theory which could correctly describe all of these phenomena was constructed over the years and is generically called ‘quantum mechanics’. In this theory, observables like particle position or energy do not have definite values anymore; these observables have a probability-like amplitude. The ‘quantum’ refers to the fact that certain observables can only take (a superposition of) discrete, quantized values in this theory.

At this moment, a theory for three out of four known fundamental forces in nature has been formulated: the electro-magnetic force and the weak and strong nuclear forces. Only the force of gravity remains “unquantized” as of this day. Yet one cannot consistently combine classical and quantum theories, so the current theories of general relativity and quantum mechanics are not complete. Hence physicists are looking for a quantized version of the theory of gravity. For more details on the subject of quantization, we refer to chapter 5.

1.3 The polygon model

In 3 dimensions, for solutions of the Einstein equations without cosmological constant, curvature of space-time does only occur locally at points where there is mass. Everywhere where space is empty, it is (locally) flat. This doesn’t mean however that things become trivial, because we can still have global non-trivial curvature effects.

The polygon model for 2+1-dimensional gravity makes clever use of this fact. We can model the spatial part of space-time as a set of polygons glued together. Inside each polygon space is simply flat, but these polygons can be glued together to form a two-dimensional spatial surface with non-vanishing two-dimensional curvature and non-trivial topology. We could for example create a cube from six four-sided polygons. The polygon model is explained in more detail in chapter 4.

There are other models for 2+1-dimensional gravity. Two formulations that are closely related to each other and the polygon formulation are the second order ADM formulation with York time by Moncrief et al. [14, 2] and the first order Chern-Simons formulation by Witten et al. [19, 2]. On a classical level, these formulations are equivalent. The quantizations of these formulations, as far as they exist, yield different results though. Witten’s formulation gives a ‘frozen time’ picture and Moncrief’s formulation can only be explicitly quantized in the genus 1 case.

2 Notation and conventions

In the polygon model, the fundamental variables are the lengths and boost parameters of the edges between polygons. These polygons cover a spatial slice of space-time. Boost parameters are the generators of Lorentz transformations between different polygons. Explicitly a boost η is related to the speed v of a Lorentz transformation by

$$\begin{aligned}\tanh(\eta) &= v, \\ \cosh(\eta) &= \gamma(v), \\ \sinh(\eta) &= \gamma(v) v,\end{aligned}\tag{2.1}$$

where as usual we have $\gamma(v) = \frac{1}{\sqrt{1 - (\frac{v}{c})^2}}$ and we normalize $c = 1$.

The boost parameters of edges can be viewed as Lorentz transformations in the specific direction perpendicular to that edge. We can more generally consider boosts in all directions together with spatial rotations. These form the (Lie) group of Lorentz transformations: we can compose any two elements to get another Lorentz transformation. We write $O(2, 1)$ for the group of Lorentz transformations in three-dimensional space-time. This group can be generated¹ by the three basic transformations of a rotation and boosts in the x and y -direction:

$$\begin{aligned}L_r(\alpha) &= \begin{pmatrix} 1 & 0 & 0 \\ 0 & \cos \alpha & -\sin \alpha \\ 0 & \sin \alpha & \cos \alpha \end{pmatrix}, \\ L_x(\eta) &= \begin{pmatrix} \cosh \eta & \sinh \eta & 0 \\ \sinh \eta & \cosh \eta & 0 \\ 0 & 0 & 1 \end{pmatrix}, \\ L_y(\eta) &= \begin{pmatrix} \cosh \eta & 0 & \sinh \eta \\ 0 & 1 & 0 \\ \sinh \eta & 0 & \cosh \eta \end{pmatrix}.\end{aligned}\tag{2.2}$$

¹Actually this will only generate the identity component $SO^+(2, 1) \subseteq O(2, 1)$, but this will be sufficient for our purposes; see appendix A for more details.

As generators of Lorentz transformations, boosts have the nice property of additivity:

$$L_x(\eta_1) L_x(\eta_2) = L_x(\eta_1 + \eta_2). \quad (2.3)$$

We will denote boosts by Greek letters from the middle of the alphabet (η, μ, ν, \dots), angles by Greek letters from the start ($\alpha, \beta, \gamma, \dots$) and lengths by l, m, n, \dots

In the polygon model, we will frequently encounter hyperbolic functions of the boosts and trigonometric functions of angles. To keep formulas short and clear, the following notation will be used:

$$\begin{aligned} v_i &\equiv v_{\eta_i} \equiv \tanh(\eta_i), \\ \gamma_i &\equiv \gamma_{\eta_i} \equiv \cosh(2\eta_i), \\ \sigma_i &\equiv \sigma_{\eta_i} \equiv \sinh(2\eta_i), \\ c_i &\equiv c_{\alpha_i} \equiv \cos(\alpha_i), \\ s_i &\equiv s_{\alpha_i} \equiv \sin(\alpha_i). \end{aligned} \quad (2.4)$$

Note the extra factor 2 in the definition of γ and σ . Furthermore, when the specification of a variable is obvious from the subscript index, then this shorter notation will be used.

Boosts, angles and lengths will sometimes be indexed along the border of a polygon and sometimes along a vertex. To distinguish between those, we will label the former with indices i, j, k and the latter with indices a, b, c . Boosts and angles with the same index are related in different ways for those cases. At a vertex, a boost and its opposite angle have the same index, while along a polygon an angle and the boost of the counterclockwise following edge have the same index. See figures 2.1 and 2.2. Note that when edges and/or vertices have to be numbered, this will always be in a counterclockwise orientation.

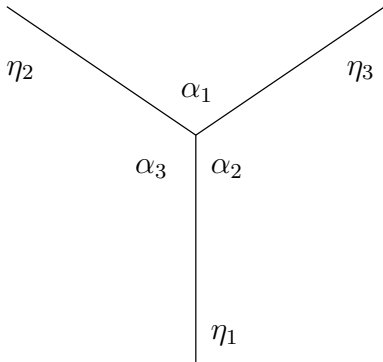


Figure 2.1: Labels of edges and angles at a vertex.

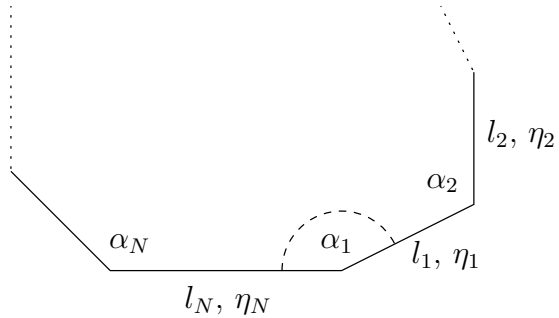


Figure 2.2: Labels of edges and angles along a polygon.

Furthermore we see that indices along a polygon are cyclic. In computations we will therefore always implicitly interpret the index numbers modulo N (N being the number of vertices and edges of the polygon). For example, we have that $\eta_0 = \eta_N$. An exception to this rule will be made for quantities that are sums over ranges of indices, as a sum over the empty range is truly different from a sum over the full cycle. For example, the sum of angles up to index j as defined in (4.6): here we interpret

$$\theta_0 = \sum_{i=1}^0 \pi - \alpha_i = 0 \quad (2.5)$$

instead of $\theta_0 = \theta_N$.

The model has a phase space consisting of a set of edge lengths and boosts (l_i, η_j) . The Poisson brackets are defined on this phase space as

$$\{l_i, \eta_j\} = \frac{1}{2} \delta_{ij}, \quad (2.6)$$

where the indices i, j run over all edges.

The phase space of this model is larger than the physical phase space. This is reflected by the presence of algebraic constraints on the phase space variables. These define a subspace of the complete phase space by imposing $C(l, \eta) = 0$ for all constraints C . When dealing with constraints, we use the ‘ \approx ’ sign to indicate an equality, that holds only on this constraint surface and not necessarily on the whole phase space. Thus by definition a constraint function $C(l, \eta)$ satisfies

$$C(l, \eta) \approx 0. \quad (2.7)$$

The polygons that together make up a ‘tessellation’, can be viewed as a graph structure, consisting of faces (the polygons), edges (the polygon edges) and vertices (the points where three or more edges join). The sets of these faces, edges and vertices will be denoted by F , E and V respectively. Single elements we denote by $f \in F$ and the number of elements by $\#F$. See section A.1 for some more details.

A note on signs

Some of the definitions used in this thesis differ by a minus sign from referenced works or conventions; unfortunately it is not possible to choose definitions to be simultaneously convenient, according to conventions and equal to all referenced works. To keep things clear, we give a (hopefully complete) list of differences.

The Poisson bracket has a relative minus sign with respect to the definition in [8]; it is chosen to have the same sign as the standard definition. Related to that is the definition of the time evolution of a classical quantity (function on phase space) as

$$\dot{f} = \{ f, H \}, \tag{2.8}$$

which is also according to normal conventions and opposite to the definition used in [8] and related papers.

Boosts have the same sign as in [8]: contracting edges have positive boosts. This looks a bit like a counter-intuitive choice, but is necessary to get the right Hamiltonian flow for our choice of signs in (2.6), (2.8) and the Hamiltonian.

We use the space-like $(-, +, +)$ sign convention for the metric.

3 Representing gravity

Before we can start to think about the quantization of gravity in arbitrary dimensions, we first have to choose a way to represent gravity. We would like to be able to formulate gravity within the framework of Lagrangian or Hamiltonian mechanics. Or in other words, we want choose a set of variables that fully describe a state of the system and then formulate the equations of motion on those states.

We must note however, that a classical “state” is normally defined as a full description of the system for a given instance of time. But in the context of general relativity “a given instance of time” is a priori not an unambiguous statement to make: there is no unique time coordinate, because coordinate diffeomorphisms are a symmetry of the system.

In the next section we will introduce a way to split time and space in general relativity, which then makes it possible to formulate general relativity in a Lagrangian and then Hamiltonian formulation of gravity.

3.1 Foliation of space-time

Before trying to split off time, we first have to give a mathematical description of a space-time. There are two well known choices of fundamental variables to describe a general space-time. We will use the standard choice of taking the metric $g_{\mu\nu}(x^\sigma)$ as field variable. There is however an alternative formulation, known as ‘first order formalism’ in which a set of orthonormal vectors e_μ^a (called ‘dreibein’, ‘vierbein’ or in arbitrary dimensions ‘vielbein’) together with an internal connection is chosen as fundamental variables. This description relates to the standard metric description via

$$\eta_{ab} e_\mu^a e_\nu^b = g_{\mu\nu}. \quad (3.1)$$

In space-time dimension n , η_{ab} is a diagonal matrix with signature $(1, n-1)$, which expresses the fact that the e_μ^a are a local orthonormal set of vectors.

A space-time can mathematically be specified in a very general manner as a differentiable manifold M with a metric g on it, often denoted as a (pseudo-)

Riemannian manifold (M, g) . In the following, we will be dealing with a pseudo-Riemannian manifold of signature (1,2).

We now want to formulate the theory in a Hamiltonian formalism, which can later be used as a starting point for canonical quantization. For this, we will choose an explicit time coordinate and introduce the concept of a global foliation of space-time. This can be seen as a continuous set of slices of space-time, where the chosen time parameter labels the different slices; time has a fixed value on the whole of each slice, see figure 3.1. To this end, we introduce a time function T on M , associating with each point in M a unique time t . This function should be sufficiently well-behaved such that its original $\Sigma_t = T^{-1}(t)$ for each instant of time is a submanifold of M , which is spatial. It must also be a monotonically increasing function along all timelike curves.

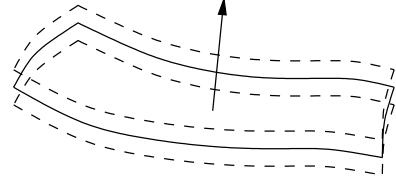


Figure 3.1: A foliation: the arrow indicates the direction of time.

The process above amounts to a partial choice of space-time¹ coordinates: we have chosen (only) a time coordinate, which slices the manifold into a set of submanifolds of equal time. Note however that this “time” is not necessarily the proper time for a local observer! This complete set of submanifolds we now call a ‘time foliation’ of the manifold M . Note that there is no unique foliation: any time function T that satisfies some regularity properties will suffice and give a different foliation.

Now that we have a time foliation, we want to pick a set of configuration variables that for a given time t specify the state of the system, just like a function $x(t)$ would describe the state (position) of a pointlike particle for a given time t . Heuristically we can say that the system is the metric on the space-time manifold M and at a given instant of time t , it is given by a spatial slice Σ_t with the restricted metric. The configuration variables for the complete manifold are given by $g_{\mu\nu}$ and for a fixed time t by restricting the metric to Σ_t and only looking at the space-space part of the metric: that is the part needed together with Σ_t to describe the state of space-time at time t . We also need to specify the conjugate momenta to get a complete set of initial conditions.

When we choose a complete set of space-time coordinates, we can make this choice of configuration variables explicit by defining

$$g_{\mu\nu} = \begin{pmatrix} -N^2 + N_k N^k & \tilde{g}_{ij} N^i \\ \tilde{g}_{ij} N^j & \left(\tilde{g}_{ij} \right) \end{pmatrix}. \quad (3.2)$$

¹One must be careful to make the distinction between coordinates that map space-time and coordinates that describe the state of the gravity system (which we will refer to as ‘configuration variables’).

The N , N^i and \tilde{g}_{ij} are functions of space-time that can be read off from the explicit form of $g_{\mu\nu}$ in the chosen space-time coordinates. We have chosen time to be a global timelike coordinate function, so this implies that $g_{00} < 0$ and also that the symmetric submatrix \tilde{g}_{ij} for the other spatial coordinates is non-degenerate and the entries $\tilde{g}_{ij} N^i$ thus well-defined.

The function N is in the literature (see e.g. [2, p. 12]) referred to as the ‘lapse function’: it specifies the rate that clocks tick with respect to the chosen time coordinate. The functions N^i are called the ‘shift functions’ and specify the displacement of spatial coordinates, when we make a small displacement perpendicular to the surface Σ_t . The matrix \tilde{g}_{ij} can be viewed as a metric on the submanifold Σ_t and thus describes the state of the system (to be compared to the position x in a one-particle classical mechanical system).

Thus far, we have not yet made any specific choice of space-time coordinates, except for the fact that we demanded a global time coordinate. The only thing we have done is to make an explicit separation of the time from the space coordinates to allow for a treatment of the theory within a Lagrangian and Hamiltonian framework. This decomposition is known as the Arnowitt-Deser-Misner (ADM) formalism.

3.2 Hamiltonian formulation

Using the ADM decomposition, we can write down the action of general relativity and transform it to a Hamiltonian formulation. We will here give an outline of this procedure, to give some insight in the intricacies that will also show up in the polygon model. More details can be found e.g. in reference [2].

The action of general relativity in three dimensions is given by

$$I = \frac{1}{16\pi G} \int d^3x \sqrt{-|g|} (R - 2\Lambda) \quad (3.3)$$

in the absence of external matter or fields. We normalize $16\pi G = 1$ and set the cosmological constant $\Lambda = 0$ from here on.

Inserting the ADM decomposition of the metric, this action can be rewritten as an integral over time t of a Lagrangian L , with

$$L = \int_{\Sigma_t} d^2x N \sqrt{|\tilde{g}|} \left[\tilde{R} + K_{ij} K^{ij} - (\tilde{g}^{ij} K_{ij})^2 \right]. \quad (3.4)$$

Here \tilde{R} is the Ricci scalar corresponding to \tilde{g} and K_{ij} is the extrinsic curvature of Σ_t embedded in M . In principle there are also some boundary terms from partial

integration, but these cancel because the spatial slice is compact. The integrand in (3.4) we denote by \mathcal{L} , the Lagrangian density.

Now we have a standard Lagrangian system and can make a transformation to canonical momenta, which yields

$$\pi^{ij} = \frac{\partial \mathcal{L}}{\partial (\partial_t \tilde{g}_{ij})} = \sqrt{|\tilde{g}|} \left[K^{ij} - \tilde{g}^{ij} (\tilde{g}_{ab} K^{ab}) \right], \quad (3.5)$$

$$I = \int dt \int_{\Sigma_t} d^2x \left(\pi^{ij} \partial_t \tilde{g}_{ij} - N \mathcal{H} - N_i \mathcal{H}^i \right) \quad (3.6)$$

$$\text{with} \quad \mathcal{H} = \frac{1}{\sqrt{|\tilde{g}|}} \left[\pi_{ij} \pi^{ij} - (\tilde{g}_{ij} \pi^{ij})^2 \right] - \sqrt{|\tilde{g}|} \tilde{R}, \quad (3.7)$$

$$\mathcal{H}^i = -2 \tilde{\nabla}_j \pi^{ij} \quad (3.8)$$

The complete Hamiltonian, given by

$$H = \int_{\Sigma_t} d^2x \left(N \mathcal{H} + N_i \mathcal{H}^i \right), \quad (3.9)$$

is now a linear combination of constraints, because the functions N, N^i do not have any equations of motion associated with them and thus act as Lagrange multipliers for $\mathcal{H}, \mathcal{H}^i$: the variation of the action (3.7) with respect to N, N^i yields $\mathcal{H} = 0, \mathcal{H}^i = 0$.

3.3 Reduction of phase space

We have found that in the Hamiltonian formulation we are left with constraint functions. This means that the real dynamics of the system takes place only in a subspace of the full phase space that we had chosen initially.

We started with a configuration space Q of all metrics \tilde{g}_{ij} on a spatial slice Σ_t and the corresponding phase space of canonically conjugate pairs $(\tilde{g}_{ij}, \pi^{kl})$. To get a description of only the true physical degrees of freedom, we have to reduce this phase space. This is done by first solving the constraint functions (3.7) and (3.8).

In addition, the constraints above are first class constraints, so they generate gauge transformations. The functions \mathcal{H}^i generate coordinate transformations of the surface Σ_t , which is a well known gauge freedom of general relativity. The function \mathcal{H} generates translations in time, relating coordinates on different time slices Σ . This is in the strict sense not a true gauge transformation, because it relates configuration variables at different times. This fact is related to the problem of time in (the quantization of) general relativity [10].

Gauge transformations do not change the physical state of the system, so as a second step, we have to fix this gauge freedom to get the reduced phase space. The gauge freedom generated by the first class constraints (3.7) and (3.8) can now be removed by fixing the Lagrange multiplier functions that were still arbitrary.

The explicit work of solving the constraints and fixing the gauge is not as straightforward as it might seem from the formulation above: there is no known way to solve this in 3+1-dimensions, but in 2+1-dimensions there is [14, 19]. We will not go into the details, but with the use of Riemann surface theory one can consider the space of metrics \tilde{g} modulo diffeomorphisms and conformal factors, which is a finite dimensional space known as the moduli space \mathcal{N} of Σ . This space has dimension $6(g-1)$ when Σ has genus $g > 1$, two when $g = 1$ and zero when $g = 0$ (see also figure 4.1 for the concept of genus of a surface). The physical phase space now has twice the dimension of this moduli space $\mathcal{N}(\Sigma)$, because we still have to add the canonical momenta, which span the same number of dimensions.

Thus in 2+1-dimensions, the physical phase space of general relativity is finite dimensional, unlike the phase space we started with: that was the space of all metrics \tilde{g} and conjugate momenta, which are fields over Σ and thus infinite dimensional. For this reason, general relativity in 2+1-dimensions is sometimes called a ‘topological theory’: the true degrees of freedom do only arise from topological non-triviality of the surface Σ . This again is a reason that the polygon model works: there are no local degrees of freedom and locally space-time is flat. The formulation of the polygon model depends on this fact as we will see in chapter 4.

4 The polygon model

The polygon model is a model to describe 2+1-dimensional space-times that can be foliated by a set of spacelike Cauchy surfaces. This includes the possibility of spatially open and closed universes [5], although in the case of an open universe one has to be careful about boundary conditions at spatial infinity.

We will however only consider spatially closed universes. Thus if we take a spatial slice of our complete space-time manifold M , then this is a closed and bounded surface (so it has finite volume). More specifically, we take a space-time of the form of a product:

$$M = \Sigma \times I. \quad (4.1)$$

Here $I \subset \mathbb{R}$ is some interval of time, which may be bounded from below and/or above, depending on whether there is a big bang or big crunch respectively.

Σ is the spatial part and thus should be a compact two-dimensional surface. These surfaces are topologically completely classified. The ones that are orientable are classified by their genus g , which indicates the number of ‘holes’ in them. The simplest examples are a sphere, a torus and a ‘double torus’, see figure 4.1.

The model also allows for a finite number of pointlike, spinless particles to be added to this space-time. We have not studied this in detail and refer the reader to [8, 11] for more information.

The simplest spatial surface of a sphere is only realizable with particles. Proof for this fact can be found in [2, p. 57] or [14, p. 2912] and is based on an analysis of the moduli space of metrics on the surface Σ modulo diffeomorphisms. For the sphere this moduli space consists of one unique metric with curvature 1, which does not yield a solution to the vacuum Einstein equations. This can also be seen

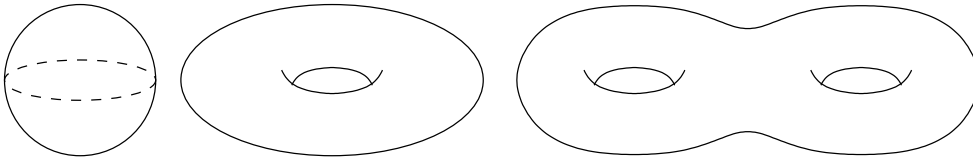


Figure 4.1: Surfaces of genus 0, 1 and 2.

from the fact that the Hamiltonian constraint can be written as in (4.11):

$$H = 2\pi\chi = 4\pi(1 - g).$$

The Hamiltonian equals minus the area of the dual graph as given in (A.10). This area cannot be negative, thus the Hamiltonian cannot be positive, which rules out the case $g = 0$.

4.1 Tessellation of the spatial surface

We are considering general relativity in 3 dimensions. This we can exploit to simplify the description of our space-time. In this case the Riemann tensor is completely determined by the Ricci tensor: one can show this e.g. by counting the degrees of freedom or explicitly [2, p. 3]:

$$R_{\mu\nu\rho\sigma} = g_{\mu\nu} R_{\rho\sigma} + g_{\nu\sigma} R_{\mu\rho} - g_{\nu\rho} R_{\mu\sigma} - g_{\mu\sigma} R_{\nu\rho} - \frac{1}{2} (g_{\mu\rho} g_{\nu\sigma} - g_{\mu\sigma} g_{\nu\rho}) R. \quad (4.2)$$

This means that in a region of space-time with no matter ($T^{\mu\nu} = 0$), the Einstein equations effectively reduce to $R_{\mu\nu} = 0$ and determine that space-time is locally flat. Thus everywhere we can locally choose a Minkowski coordinate system.

Given this space which is locally Minkowski, we can also easily choose a spatial slice that is locally flat too. This will induce a local coordinate system from the three-dimensional Minkowski space to our two-dimensional spatial slice Σ_t . We cannot in general extend this coordinate system to our whole spatial surface: our space is compact, so when we try to extend our flat coordinate system from a certain starting point, we will run into parts of space where we had already defined coordinates. These do not necessarily have to match; while we have extended our coordinates and run into a “charted” part of space, we might have gone around a non-contractible loop in Σ which has a non-trivial holonomy. A simple example is a toroidal spatial surface which expands uniformly in one of its fundamental directions: when we walk along a loop in this direction and return to our starting point, the coordinates fail to match by a Lorentz boost of the speed of contraction or expansion.

We can however choose a coordinate system at some point(s) of our spatial surface and extend it as far as possible. After doing this, we will be left with several regions of flat space which, glued together at their boundaries, form the complete spatial surface again. We will call such a set of flat coordinate patches a ‘tessellation’. Notice that at points where regions of space are glued together, the spatial surface will in general not be flat. The underlying three-dimensional Minkowski space-time is flat, but at points where three or more spacelike slices join, the two-dimensional surface will in general have a curvature of delta distribution type. See figure 4.2 for an example.

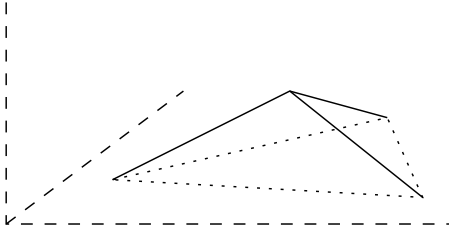


Figure 4.2: Curvature at a vertex of three joined 2D surfaces in a flat 3D background.

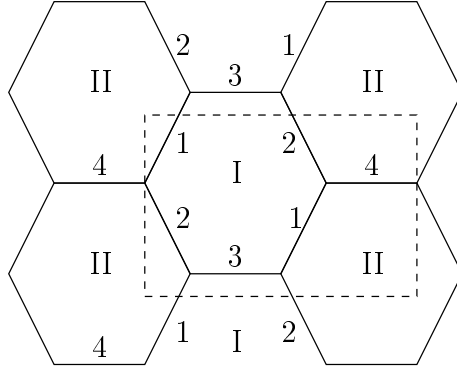


Figure 4.3: Tessellation of a torus by 2 polygons, labelled I and II.

This is a tessellation of a spatial surface at one fixed value of the time coordinate. The coordinate systems of the different patches should therefore obey some boundary conditions, such that there is no time difference when traversing a boundary and also time should run equally fast on both sides. This implies that the boundary should move perpendicular to its orientation in the coordinate frames on both sides, which yields that a boundary must be a straight line and its velocity be of same size and opposite direction in the neighboring coordinate frames (see [5, p. 1336] for a more detailed discussion).

An example of a tessellation is given in figure 4.3: the dashed lines show a fundamental domain of the torus (with the usual identification of opposite sides) and two 6-sided polygons covering this torus. The two polygons are labelled I and II and the different edges are labelled 1 to 4. Notice that these polygons have a number of edges in common with each other and also with themselves.

Thus our tessellation consists of a number of polygon coordinate patches with sides that have to be identified. The sides of these polygons have well-defined lengths within the coordinate frames of the respective polygons. These should however match the length of the edge as seen in the coordinate frame on the opposite side of the boundary (because the metric should be continuous). Therefore these boundary edges have a unique, well-defined length l .

Besides that, we can assign a boost parameter to each edge. This boost is $\eta = \tanh^{-1}(v)$, where v is the speed of the edge in its neighboring coordinate frames. The speed and boost have a positive sign when the edge moves inward, thus v is the speed at which the edge contracts the polygon. This speed is uniquely defined, because an edge must expand or contract with the same speed in the coordinate frames on both its sides. The Lorentz transformation relating two neighboring coordinate frames is then given by a boost of 2η : first a boost from one frame to the rest frame of the edge and then again a boost from the edge rest frame to the other coordinate frame.

4.2 Vertex relations

We have made a tessellation of our spatial slice with polygons. These polygons exactly cover this spatial slice, so boundaries (‘edges’) of these polygons have to be identified where they are “glued together”.

Besides that we also have ‘vertices’: points where three or more edges join. As was stated earlier, space-time is locally flat. This should also hold at vertices. To express the curvature located at a vertex, we can write down the holonomy around that vertex: the change a vector undergoes when it is being parallel transported around that vertex.

We can explicitly write down the complete holonomy of going around the vertex using the Lorentz matrices (2.2). Going around in anti-clockwise orientation, we label the polygons at the vertex $i = 1 \dots n$ and define α_i as the angle that polygon i makes at the vertex and $2\eta_i$ the boost between polygon i and polygon $i+1 \bmod n$. Now going around means successively making a rotation $L_r(\alpha_i)$ and a boost $L_x(2\eta_i)$ for each polygon.¹ This should be equal to the identity operation, as space-time must be flat at the vertex point, thus we have

$$\prod_{i=1}^n L_r(\alpha_i) L_x(2\eta_i) = \mathbb{1}. \quad (4.3)$$

We demand that at a vertex always exactly 3 polygons join. This is always possible by choosing a suitable tessellation and will allow us to express the angles in terms of the boosts. For later convenience, we now choose the indices of boosts and angles in a more symmetric fashion as in figure 2.1. When we rewrite (4.3) to a form with 3 matrices on the left and the right side and then explicitly work out the equations, we get:

$$s_1 : s_2 : s_3 = \sigma_1 : \sigma_2 : \sigma_3, \quad (4.4a)$$

$$0 = s_1 c_2 + \gamma_2 s_3 + c_1 s_2 \gamma_3, \quad (4.4b)$$

$$c_1 = c_2 c_3 - \gamma_1 s_2 s_3, \quad (4.4c)$$

$$\gamma_1 = \gamma_2 \gamma_3 + c_1 \sigma_2 \sigma_3 \quad (4.4d)$$

and all cyclic permutations of the indices. Here we used the notation as in (2.4). As in the literature, we will refer to these as the ‘vertex relations’. These equations are not independent [4] nor have we given the same set as originally

¹Remember that the transformation between two neighboring polygons goes with twice the boost of the edge. Furthermore the precise choice of signs and L_x or L_y depends on the explicit choice of coordinates in the polygons and orientation of the holonomy, but this does not affect the resulting equations. This can be seen from the fact that the system has space and time mirror symmetry.

given by 't Hooft in [5], but they are complete in the sense that they are equivalent to the full set of equations determined by (4.3).

These equations now give us expressions for the angles of polygons in terms of boost parameters or vice versa. To determine the angles one can for example rewrite equation (4.4d) and take the inverse cosine. This does not yet determine the angle uniquely, but with the help of equation (4.4a) it does. There is the extra fact that at most one of the three angles at a vertex can be larger than π , because if there would be two angles larger than π , there would be points that show up in the coordinate systems of both polygons [7]. This then determines the sign of the sines of the angles at each vertex.

4.3 Constraints

We now have a representation of a 2D spatial slice of the 2+1D space-time manifold M in terms of one or more polygons, glued together at their edges. A configuration of such a spatial slice is described in terms of the lengths l_i and boost parameters η_i of all edges together with the graph structure of all these edges.

The l_i, η_i however cannot take all possible values in \mathbb{R}^{2N} . Besides the fact that all lengths have to be positive ($l_i \geq 0$), there are some other, more complicated constraints.

Firstly the boosts at each vertex have to obey a triangle inequality. For each triple of boosts at one vertex and each permutation thereof, the following must hold:

$$|\eta_a| + |\eta_b| \geq |\eta_c| \quad (4.5)$$

This can be deduced from vertex relation (4.4d). A more geometrical argument is as follows: when going around the vertex, we are Lorentz boosted three times, but we should return to our original rest frame. The resulting boost of two boosts is at most the sum of the boosts, exactly when they are collinear. So the sum of lengths of each two boosts must be greater than the third to be able to close the holonomy. This is analogous to the case of Galilean transformations when we replace the boosts by normal velocities.

Secondly there is a set of constraints for each polygon. Geometrically these are easy to formulate: each polygon must close. This means that the angles and edge lengths must be such that when going around the border of a polygon and keeping track of the relative coordinates, that one must end up exactly where one started and the sum of the angles must be 2π .

As the angles can be expressed in terms of the boosts, we can explicitly express these constraints in terms of the model variables l_i, η_i . For a fixed polygon, let

us number the lengths, boosts and angles according to figure 2.2.

We first define the angle between edge j and the horizontal (edge N) by

$$\theta_j = \sum_{i=1}^j \pi - \alpha_i. \quad (4.6)$$

Using this we can write down the angular and closure constraints as

$$C_\theta = \theta_N - 2\pi = \sum_{j=1}^N (\pi - \alpha_j) - 2\pi \approx 0, \quad (4.7a)$$

$$C_z = \sum_{j=1}^N l_j \exp(i\theta_j) \approx 0. \quad (4.7b)$$

The closure constraint C_z is written using an implicit complex coordinate system in the polygon. This way of writing is obviously equivalent to formulating two real-valued constraints for the x and y direction. We will refer to the second constraint as the ‘complex constraint’ as in [18].

4.4 Dynamics

From the definition of our length and boost parameters, we can find the evolution of these parameters. The boosts do not change in time, except when transitions take place. The lengths however do change. A geometrical analysis shows that the length change of an edge gets a contribution from the vertices at both its sides equal to

$$\frac{dl}{dt} = -\frac{\tanh(\eta_1) \cos(\alpha_3) + \tanh(\eta_2)}{\sin(\alpha_3)} = -\frac{v_1 c_3 + v_2}{s_3}, \quad (4.8)$$

where index 1 numbers the edge under consideration and indices 2 and 3 may be interchanged (there is mirror symmetry).

We can also look at the evolution of the system in the Hamiltonian formulation. The Hamiltonian is given by the total two-dimensional curvature of the spatial slice. Curvature is only present at vertices and is given there by the deficit angle, thus

$$H = \sum_{v \in V} \left(2\pi - \sum_{i=1}^3 \alpha_{v,i} \right). \quad (4.9)$$

We can see that this Hamiltonian is a constraint: on the one hand, it is the integral over the scalar curvature, which is only dependent on the Euler characteristic χ

(see formula (A.2)) by the Gauss-Bonnet theorem:

$$H = \int_{\Sigma} d^2x \sqrt{\tilde{g}} \tilde{R} = 2\pi \chi = 4\pi(1-g). \quad (4.10)$$

On the other hand we can see that it is equal to the sum of all angular constraints, using the Euler characteristic of the graph:

$$\begin{aligned} 0 &= \sum_{f \in F} (C_{\theta}^f - 2\pi) \\ &= - \sum_i \alpha_i + (3\#V - 2\#F)\pi \\ &= \sum_{v \in V} \left(2\pi - \sum_{i=1}^3 \alpha_{v,i} \right) + (\#V - 2\#F)\pi \\ &= H - 2\pi \chi. \end{aligned} \quad (4.11)$$

In the last step we made use of the trivalence of the vertices by plugging in the relation $3\#V = 2\#E$. See page 7 for notation.

The Hamiltonian now generates evolution of the system by

$$\begin{aligned} \frac{dl_i}{dt} &= \{l_i, H\}, \\ \frac{d\eta_i}{dt} &= \{\eta_i, H\}. \end{aligned} \quad (4.12)$$

To explicitly calculate this, we need a symplectic structure on phase space. A symplectic structure defines Poisson brackets and it is uniquely determined by the Poisson brackets between the fundamental variables. In our case it turns out that the evolution of the boosts and lengths exactly matches the evolution generated by the Hamiltonian if we choose the symplectic structure to be (2.6):

$$\{l_i, \eta_j\} = \frac{1}{2} \delta_{ij}.$$

The Hamiltonian time evolution of the boost parameters can immediately be seen to match that of the geometrical picture: in both cases it is zero. For the geometrical picture it was chosen this way by letting time run equally fast everywhere in each polygon. For the Hamiltonian evolution, we see that it follows from the fact that H only depends on the boost parameters.

4.5 Transitions

Given the results of the previous section, the evolution of the system looks simple: the boosts and angles are fixed and the lengths change linearly in time. It turns out that things are not that simple: there is a complicating factor coming from the constraint that the model parameters must describe a true tessellation. This means that edge lengths must be positive and polygons must be true, non-self-intersecting polygons.

As a side remark, it must be noted that strictly speaking, polygons may be self-intersecting, but only in such a way that they can be embedded in a non-self-intersecting way on some two-dimensional surface, see [6]. This can be formulated as follows: if a polygon intersects itself then this will generate a transition if and only if a new triangle is formed and the winding number of points that will lie in the triangle decreases with respect to the oriented boundary of the polygon. If the winding number of these points decreases, then these points are on the outside of both parts of the polygon boundary that cross and thus would start to show up in two different places in polygon coordinate charts.

Figures 4.4 and 4.5 show two polygons that both seem to self-intersect. In the first a transition will split the polygon into two parts when the vertex hits the horizontal edge. The winding number of points in the new triangle decreases from 0 to -1 . In the second figure, no transition will take place when the vertex crosses the edges as indicated.

Returning from this digression, we now have essentially two transitions that can happen: an edge collapsing to zero length (the top left diagram in figure 4.6) and a vertex hitting an edge (top right). There are some special cases of these two transitions. If an edge is part of a triangular polygon, then this whole polygon will disappear when the edge length goes to zero. This is due to the fact that boosts and angles are constant and thus a triangle will scale to zero size when one of its edges does. This can also happen with two neighboring triangles (but

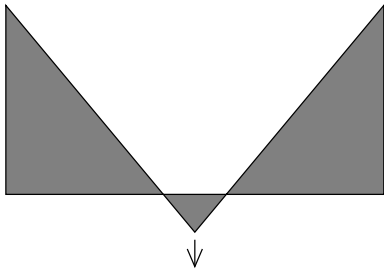


Figure 4.4: A truly self-intersecting polygon.

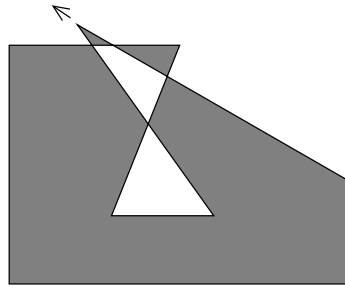


Figure 4.5: A superficially self-intersecting polygon.

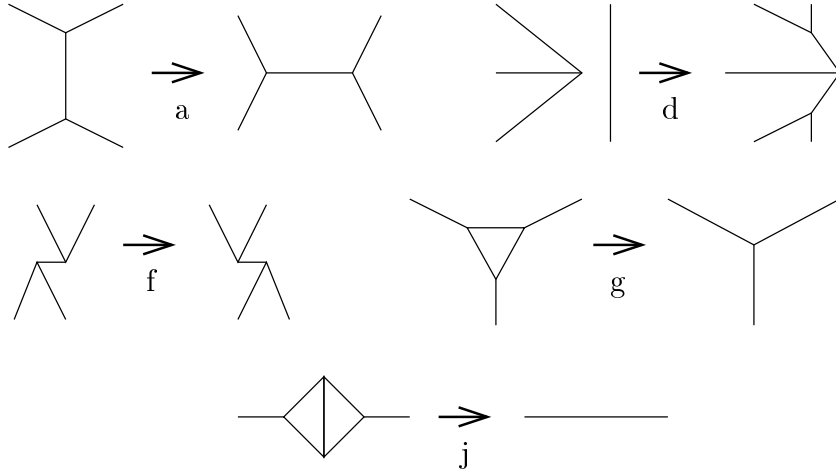


Figure 4.6: All possible polygon transitions without particles, labelled as in [6].

not with three, as they would together close the spatial slice, but violate initial conditions). See the middle right and bottom diagrams of figure 4.6. Furthermore we have a special case when an edge shrinks to zero, but the angles are such that it starts growing again, but with angles changed by π (called a ‘grazing transition’ in the literature); see the middle left diagram of figure 4.6.

There are a few more possible transitions when one allows particles in the model. For the full set of transitions including those with particles we refer to [6].

Now if we have a set of initial conditions that satisfy the constraints, we can calculate the time evolution. This is in first instance given by only the length change of the edges. But after a certain amount of time, the polygon configuration may have changed in such a way that a transition as depicted in figure 4.6 is about to take place. This will not only change the graph structure as indicated, but also the model parameters will change. One can find these by demanding that the parameters after the transition should be consistent with those before and that they should obey the vertex relations: space-time must stay flat.

A potential problem now arises: when a transition takes place, we switch to a different graph structure with a different set of edges and thus a different phase space to describe the system. The number of edges does not need to be the same, so the dimension of the phase space can change during a transition. The dimension of the physical phase space does not change (as expected). This we can see from counting degrees of freedom and constraints. The Euler characteristic (see section A.1) is

$$\chi(\Sigma) = \#V - \#E + \#F \quad (4.13)$$

and is constant for a given topology of Σ . From the trivalence of the vertices, we

obtain $3 \#V = 2 \#E$. This together gives us the relation

$$\#F - 3 \#E = \text{constant}, \quad (4.14)$$

which does not depend on the specific structure of the graph. Now two degrees of freedom are associated with each edge. Each polygon on the other hand introduces three constraints. And as we have seen in section 3.3, each constraint generates a complementary gauge degree of freedom. So each polygon amounts to a total of six unphysical degrees of freedom in the full phase space, which exactly cancels the extra degrees of freedom added by the edges.

4.6 Constrained dynamics

With the addition of transitions, we now have a complete description of the (classical) dynamics of the system: given a set of initial conditions, we can uniquely determine the evolution of the system. This system must not only be uniquely defined, but also be well-defined. For this we have to check that all constraints (equalities and inequalities) are preserved under the evolution of the system.

4.6.1 Equality constraints

We want to check that time evolution preserves the constraints, which amounts to checking that $\{C, H\} \approx 0$ for all constraints. This follows trivially for the angular constraints, because they do not depend on the lengths. The calculation for the complex constraints is not straightforward, but also gives $\{C_z, H\} \approx 0$: see chapter 6 for the details.

Besides this, one must also check that the constraints are preserved during transitions. This turns out to be relatively simple for the complex constraint: during transitions of the type where an edge length reduces to zero (transitions a, f, g, j in figure 4.6), only edges with length zero are removed and created. Thus these do not affect the complex constraints. Also in the case of transition type d, the complex constraint is conserved: the new lengths of the split edges are by construction chosen to match the complex constraint.

The angular constraints are also preserved under transitions. The best way to understand this is by looking at the dual graph (see appendix A and [4, 13]). This graph is constructed by mapping vertices into faces and vice versa. Edges are mapped to themselves and to each edge in the dual graph we associate an (oriented) length $\tilde{l} = 2\eta$, where η was the boost of the edge in the original graph. To each angle α we associate an angle $\tilde{\alpha} = \pi - \alpha$ in the dual graph as shown in figure 4.7.

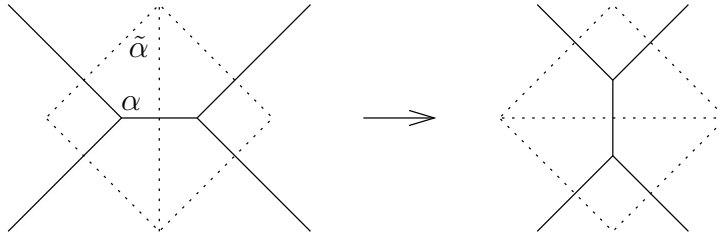


Figure 4.7: An edge transition and the dual graph (dotted lines).

Now a transition will also induce a corresponding transition in the dual graph. As explained in appendix A, the dual graph (with the mapping of edge lengths and angles) can be embedded in the hyperbolic plane. From the transitions in the dual graph, it can now be shown that the angular constraints are preserved

Making an edge transition of type a (figure 4.6) is now a matter of removing an edge in the dual graph and replacing it by the opposite edge within the quadrilateral just created, as in figure 4.7. This dual graph is embedded in hyperbolic space, where every point has a full 2π neighborhood (as in flat space). Each neighborhood of a vertex in the dual graph is also fully covered before the transition, as can be deduced from the angular constraint of the polygon corresponding to that vertex.

The other transitions can be dealt with in a similar fashion: the angular constraints are encoded in the dual graph as vertices containing a 2π neighborhood and making the corresponding transition in the dual graph does not change this, thus the transition should preserve the angular constraint. We have not checked this explicitly and there might arise some problems, when mixed vertices are involved, see section A.3.

4.6.2 Inequality constraints

In section 4.3 we saw that there are also some inequalities to be satisfied, namely, lengths must be positive and the boost parameters must obey triangle inequality (4.5). This raises some problems when trying to find a quantized version of this model.

In a standard Hamiltonian formulation, we have a configuration space Q and a state of the system is given as a point in the cotangent space T^*Q . Normally Q is chosen to consist of the positions (lengths in our case) and then elements in the vector space T_q^*Q are the momenta (the boosts in our case). We now face the problem that the Hamiltonian is only defined for those boosts that satisfy the triangle inequality, and thus H is not a function on the whole phase space T^*Q .

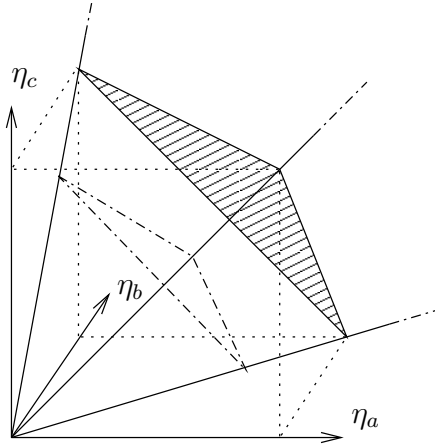


Figure 4.8: The restriction of boosts by the triangle inequalities.

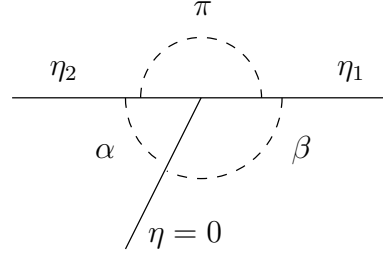


Figure 4.9: Parameters at a vertex with one zero boost.

In figure 4.8, a picture is given of the triples of boosts (η_a, η_b, η_c) at one vertex that satisfy these inequalities. These are the triples within the triangles like the one shaded in the figure, stretching out radially. Note that the picture does only display the triples in the first octant of \mathbb{R}^3 (all boosts positive), so the full picture should be mirrored in three planes. Moreover, it only shows the constraints from one vertex; each edge is connected to two vertices, making the complete set of inequalities more complicated.

Special care has to be taken at the boundary of the inequalities, when they are exactly satisfied. Here we can distinguish two cases according to whether one of the three boosts η_a, η_b, η_c is zero or not. If none of the three is zero, the angle opposite to the largest boost is zero, which does not correspond to an acceptable tessellation.

If one of the boosts is zero, the other two must be equal (also in sign) and a degree of freedom in the boosts is replaced by a degree of freedom in the angles at that vertex. This can easily be seen from the geometrical picture (see figure 4.9): if one edge boost is zero, the polygons separated by that edge can be joined together as the Lorentz transformation between those polygons is trivial. Then the two other edges with boosts η_1, η_2 become one edge and thus should have the same boosts $\eta_1 = \eta_2$ and angle π between them. In this case, the angle α is not determined by the vertex relations and can be chosen freely. Given α , we have $\beta = \pi - \alpha$. If we also take $\eta_1 = 0$, the triangle inequality implies that also $\eta_2 = 0$ and the three angles are free but should add up to 2π .

This change from boosts to angles to parametrize the degrees of freedom in phase space seems to indicate that the l_i, η_j coordinates cannot cover the full phase space. The subspace not covered seems to be lower-dimensional though.

4.7 Simulation

Lastly, it must be mentioned that this polygon model has as one of its virtues that it is well suited for numerical simulation [8]. The model has an explicit description of the evolution of the system, which is finite dimensional and not in terms of differential or integral equations. This allows one to “exactly” simulate it on a computer: the exactness is only bound by the finite precision used in the simulation.

To simulate a space-time, one must first find a set of parameters that satisfy the constraints. This is in general very hard, but an explicit (but intricate) method for genus $g > 1$ has been given by Kadar and Loll in [13] using the dual-graph representation (see appendix A). A more simple approach is to start with a completely symmetric one polygon tessellation (OPT) and perturb the parameters slightly. One can then pick one boost and two lengths and solve the angular and complex constraints for those. This approach does not yield initial conditions for the full phase space however.

Now, one can simulate the polygon model by calculating the length changes \dot{l}_i from (4.8) and let time run. If this length change will result in one of the transitions in figure 4.6, one has to “stop” the simulation and perform the transition, by changing the graph structure and calculating the new parameters using the vertex relations (4.4). This can then be repeated until we either run into a big crunch, or there are no transitions taking place anymore and space expands to infinity. One can also reverse time by changing sign of all boosts, to simulate the past of a given configuration.

We mentioned that this simulation is exact up to numerical precision. Unfortunately, if the universe collapses towards a big crunch, the boosts tend to grow exponentially under transitions and precision is lost after only a couple of transitions. This inaccuracy cannot be prevented easily as the boosts are calculated using hyperbolic sines and cosines, thus making intermediate expressions roughly exponentials of the boosts and absolute errors blow up equally fast.

We have implemented a simulation program too, to gain a better understanding of the details of the model and with the hope of revealing some interesting aspects of $2+1$ -dimensional gravity for genus $g > 1$. This last goal has showed to be fairly difficult: the interpretation and visualization of simulation data is hard and especially the extraction of physical information turned out to be difficult. The observations that we made in this simulation as mentioned above, do coincide with those already made by 't Hooft in [8].

5 Quantization

The polygon model for $2+1$ -dimensional gravity is a relatively simple model, with only a finite number of degrees of freedom. Furthermore we have been able to explicitly formulate it in a Hamiltonian formalism. This raises the question whether it is possible to quantize this model. Even though a full four-dimensional quantum gravity theory would still be far away, it might give interesting indications about qualitative aspects of quantization of general relativity.

One such thing is the question whether space and/or time will become discretized. Already for this model there are different predictions: 't Hooft argues in [6] that the imaginary part of (analytically continued) lengths will be quantized and that time will be discretized. This means that the time evolution is well-defined for discretized time steps only. Waelbroeck on the other hand argues in [17] that this time discretization can be lifted by choosing an internal time: the Hamiltonian constraint is solved for one of the boosts and this boost, expressed in terms of the other boosts, will then take the role of the Hamiltonian and its conjugate edge length will take the role of time.

As already argued in the papers cited above, the quantized version of this theory might very well depend on the way we quantize. We have a set of constraints, which we can choose to first solve and only then quantize the reduced phase space. On the other hand, we can also first quantize and afterwards impose these constraints as operators in the quantum theory.

These predictions about a quantum theory of the polygon model are heavily dependent on the way one quantizes the theory. We will be concerned with finding a canonical quantization only and not consider other quantization methods like path integral quantization: canonical quantization is already a non-unique quantization scheme, that is also not guaranteed to work. Therefore we will first investigate the a priori question of whether a consistent canonical quantization exists, before further investigating the predictions of a quantized model.

5.1 General procedure

Here, we will describe what it means in a general setting to canonically quantize a classical system.

We start with a classical system with a configuration space Q , which is locally isomorphic to \mathbb{R}^n , or in other words, which is an n -dimensional smooth manifold. This also naturally defines a phase space as the cotangent space $P = T^*Q$, in which we can identify a pair of position and momentum coordinates (x, p) as the base point $x \in Q$ and $p \in T_x^*Q$ as a linear form on the tangent (velocity) vectors at x .

On this phase space in turn is defined a Poisson bracket structure, which maps pairs of functions on P to new functions on P , defined in local coordinates (x, p) as

$$\{f, g\} = \sum_{i=1}^n \left(\frac{\partial f}{\partial x_i} \frac{\partial g}{\partial p_i} - \frac{\partial f}{\partial p_i} \frac{\partial g}{\partial x_i} \right). \quad (5.1)$$

A Hamiltonian, defined as a function on the phase space, then describes the classical evolution of the system by the flow of the Hamiltonian vector field: $\chi_H = \{ \cdot, H \}$.

Now quantization amounts to the following. We want to map classical observables to quantum operators. These operators must act on wave functions in a vector space with inner product, that is, a Hilbert space. In the following, we will construct the picture bottom up; this is contrary to the way one would construct a quantum theory in practice, but allows us to specify the mathematics involved more rigorously.

We consider a Hilbert space S of wave functions mapping from the configuration space Q to the complex numbers. The inner product on this Hilbert space defines normalization of wave functions. Normally this Hilbert function space is chosen to be the square integrable functions $L^2(Q; \mathbb{C})$.

Within this Hilbert space, we consider a finite dimensional Lie group G within the set of unitary operators $U : S \mapsto S$. Such a Lie group G has a Lie algebra \mathcal{G} associated with it, which carries the standard anti-symmetric multiplication structure, called the Lie brackets, such that for all $f, g, h \in \mathcal{G}$:

$$\begin{aligned} [f, g] &= -[g, f] \\ [f + g, h] &= [f, h] + [g, h] \\ 0 &= [f, [g, h]] + [g, [h, f]] + [h, [f, g]] \end{aligned} \quad (5.2)$$

We are then looking for a set of classical observables, that is, functions on the phase space P , a Lie group and its corresponding algebra \mathcal{G} and a mapping from

these classical observables O_i to Lie algebra elements $\mathcal{O}_i \in \mathcal{G}$, for which the Poisson brackets are mapped to $-i$ times¹ the Lie brackets. In this mapping of the classical operator Poisson algebra to a Lie algebra, one normally also includes a ‘quantum deformation’. This means that these relations are modified by adding a factor like \hbar to introduce a quantum scale.

This process of canonical quantization is by no means a straightforward procedure: the choice of Hilbert space, classical operators and mapping to quantum operators is not prescribed. One must just try and see whether the choice made gives a consistent scheme.

In ordinary quantum mechanics on \mathbb{R}^n , one promotes x and p to operators, which yields the well-known commutation relations

$$[\hat{x}_i, \hat{p}_j] = i\hbar \widehat{\{x_i, p_j\}} = i\hbar \delta_{i,j} \hat{\mathbb{1}}. \quad (5.3)$$

Here we see that a quantum deformation of a factor \hbar has been added.

This is then combined with the Hilbert space $S = L^2(\mathbb{R}^n; \mathbb{C})$ of square-integrable wave functions over the positions $x_i \in \mathbb{R}^n$. The operators \hat{x}_i and \hat{p}_j are realized on this Hilbert space in the position representation as the self-adjoint operators

$$\begin{aligned} \hat{x}_i \phi(x) &= x_i \phi(x), \\ \hat{p}_j \phi(x) &= -i\hbar \frac{\partial \phi(x)}{\partial x_j}. \end{aligned} \quad (5.4)$$

5.2 Constraints in quantization

In the outline above, we have not yet talked about constraints. These do not show up in the canonical quantization of a particle: there all degrees of freedom are truly physical degrees of freedom. In the polygon model we have to accommodate constraints. This can be done in essentially two ways: we can either implement those at the classical level and then quantize, or we can first quantize the theory and only then implement the constraints quantum mechanically.

Implementing them at the classical level means that we solve the constraints classically by constructing a fully reduced phase space. Thus we have to reparametrize the phase space coordinates of the system in such a way that the constraints are fulfilled by construction.

We must be careful in solving the constraints: the theory was formulated as a generally covariant theory, which means that if we solve all constraints, we are left

¹This depends on conventions: physicists tend to add the $-i$, with the effect of the operators becoming Hermitian, thus having real eigenvalues. The operators in the Lie algebra however have to be anti-Hermitian to give unitary operators when exponentiated.

with a so called ‘frozen time’ picture. The Hamiltonian itself was a constraint in this formulation, so time evolution is a (semi) gauge transformation. This means that if we naively solve the Hamiltonian constraint, then in the fully reduced phase space, the Hamiltonian constraint is just a constant, so the Hamiltonian equations of motion become trivial. The state space of the system is then exactly parametrized by a complete set of constants of motion.

This problem of a frozen time picture can be overcome by breaking general covariance. We can introduce a time again (often referred to as ‘internal time’) by choosing a classical observable that is monotonic in the original time parameter. The simplest choice for such a parameter is one of the edge lengths. Let us label this length and its conjugate boost by (l_0, η_0) . The action

$$S[(l_0, l_i, \eta_0, \eta_i)(t)] = \int dt \left[2\eta_0 \dot{l}_0 + \sum_i 2\eta_i \dot{l}_i - u H - \sum_{f \in F} \left(v_f C_\theta^f + w_f C_z^f \right) \right] \quad (5.5)$$

then yields the correct equations of motion. We see that the Hamiltonian and all constraints have Lagrange multipliers $(u, v_f \in \mathbb{R}, w_f \in \mathbb{C})$ associated with them; the equations of motion for these multipliers result in the constraint equations, cf. (3.9). If we now solve the equation $H(\eta_0, \eta_i) = 0$ for η_0 , we obtain $\eta_0(\eta_i)$ and plugging this in the action, while substituting integration over t with l_0 , we obtain

$$S_{\text{red}}[(l_i, \eta_i)(l_0)] = \int dl_0 \left[\sum_i 2\eta_i \frac{dl_i}{dl_0} + 2\eta_0(\eta_i) - \frac{dt}{dl_0} \sum_{f \in F} \left(v_f C_\theta^f + w_f C_z^f \right) \right]. \quad (5.6)$$

We see that we have removed one pair of canonical coordinates, while solving the Hamiltonian constraint. The Hamiltonian is now given by $H_{\text{red}} = -2\eta_0$ together with the remaining constraints and their Lagrange multipliers. Also, some of the complex constraints will explicitly depend on the new time parameter l_0 .

In theory, this method of introducing an internal time will thus yield a system with non-trivial equations of motions. The explicit equations of motion will depend on the solution of $\eta_0(\eta_i)$ from $H = 0$, which is in practice hard to solve.

The other way of implementing the constraints at the quantum level comes down to first quantizing the complete phase space and then constructing quantum mechanical operators \hat{C} for each constraint C according to Dirac’s prescription. A physical wave function ϕ must then satisfy

$$\hat{C} \phi = 0. \quad (5.7)$$

Again, we are faced with the Hamiltonian constraint. If this constraint is enforced at the quantum level, we have $\hat{H} \phi = 0$, and thus that states are constant in time. If we first solve the Hamiltonian constraint as in (5.6), we have a highly complicated system, where a lot of symmetry has been removed.

5.3 Quantization of the polygon model

Given the classical formulation of the polygon model in chapter 4, we want to find a consistent choice of quantization.

The most straightforward choice as proposed by 't Hooft in [6], is to promote the canonical coordinates l_i, η_j to operators, as in standard quantum mechanics. The Poisson brackets of these variables are the same as in (5.3) (up to a factor $\frac{1}{2}$).

We now run into a problem: the Stone–Von Neumann uniqueness theorem tells us that the canonical commutation relations (5.3) have one unique representation, when \hat{x} and \hat{p} are self-adjoint operators on a separable² Hilbert space (see e.g. [16, p. 65]). This representation is the Heisenberg representation and implies that the eigenvalue spectrum of both the \hat{l}_i and $\hat{\eta}_j$ would consist of the whole real line. The spectra of these operators in the quantum theory do not correctly reflect some properties of the original classical system, namely, the inequalities for the lengths $l_i \geq 0$ and the triangle inequalities (4.5) for the boosts. We will now try to analyze whether these apparent problems can be remedied.

5.3.1 Transitions

The inequalities that lengths should be positive can be directly related to graph transitions. In the classical case, when a length would become negative, we demand that a transition takes place instead. This is because, at least classically, introducing negative lengths might give rise to all sorts of strange things like negative spatial volume or overlapping coordinate charts. These overlapping coordinates would also show up when we ignore transition d in figure 4.6; a case that is not covered by the inequalities $l_i \geq 0$.

The question is now how we want to treat this in a quantum theory. Allowing negative lengths and ignoring transitions will clearly remove the non-trivial dynamics from the model. Therefore it seems that we should also restrict the quantum mechanical system to these length inequalities and probably rule out overlapping coordinates like in figure 4.4, too.

If we try to implement transitions in the quantum theory, we face the fact that transitions change the graph structure and the coordinates of the phase space. In the case of a polygon merging or splitting transition, they even change the dimension of phase space. This poses a significant problem for the formulation of

²A topological space is separable when it has a dense subset that is countable. A Hilbert space of countable dimension is separable. If separability is not demanded, then other representations can be constructed, see [1]. In these representations either \hat{x} or \hat{p} will not be a well-defined operator, although the exponentiated form will be well-defined. The spectrum of the other operator will still be the whole real line though.

a quantized theory: how should these different phase spaces be brought together in one quantum theory?

In [6] 't Hooft suggests to make an analytical continuation of the wave functions, such that they are continuous across transitions. Implementing the constraints on the quantum level should then also ensure that the wave functions are constant under gauge transformations.

There are however not only the continuous symmetries generated by the constraints, but there is also a discrete overcounting of physical states: one and the same universe can be represented by multiple completely different (on a graph structure level) tessellations. It might be possible that these different graphs can be transformed into one another by finite gauge transformations, but this is not a priori clear.

This raises questions like whether one wants to keep those overcounted graphs on the quantum level or not and how to deal with either option. If one wants to remove this symmetry, then what should be the choice of gauge fixing? If one wants to keep these discrete symmetries, how do we construct one global Hilbert space and a proper measure on it?

For the first option, a possible way to partially solve the problem of gauge fixing is offered in [13]. There it is conjectured that every element in the physical phase space can be constructed as an OPT. This would allow one to write all multi-polygon tessellations as OPT's by a suitable gauge transformation and thus keep the phase space of fixed dimensions. Then one would either need to explicitly find this 'suitable gauge transformation', which seems a non-trivial task, or one would have to show by other means that the phase space is complete.

5.3.2 The triangle inequalities

In the construction of the polygon model, we imposed that there is no cosmological constant or matter, which implies that space-time is flat. These are sufficient conditions to obtain the triangle inequalities.

As these inequalities are inherently connected to the way the model is constructed, it seems that they should also be imposed on the quantum level; otherwise, the quantum theory would have regions that are classically forbidden and it is therefore difficult to see how a correct classical limit could emerge. Furthermore the classical Hamiltonian is only defined for those boosts that satisfy the triangle inequalities.

Each triangle inequality in itself does not restrict a single boost η_i to a certain domain, but the inequalities do couple boosts at a vertex: choosing values for two boosts at a vertex restricts the value of the third boost to a bounded domain.

Even stronger, these inequalities couple between all boosts due to the fact that each edge is connected to two vertices and all edges to each other through the graph structure of the tessellation. This is in conflict with the canonical commutation relations (5.3), because by the Stone–Von Neumann theorem, each boost η_i should have spectrum \mathbb{R} independently. This problem could be overcome, if we can find a symplectic transformation³ of the phase space that decouples the inequalities for the new coordinates.

5.3.3 Other choices of quantum variables

As laid out above, the coordinates l_i, η_j are both restricted by inequalities at the classical level, which gives problems when trying to promote them to quantum operators. A possible way to avoid this problem is to choose a different set of coordinates to be promoted to quantum operators.

We can try to reparametrize our coordinates in such a way that the inequality constraints simplify and/or decouple; or we might be able to find a reparametrization, which exactly parametrizes the part of phase space where the inequalities are satisfied.

These methods of choosing a different coordinatization of phase space can be extended to a more general way to attack the problem of these inequalities. We can choose a set of phase space functions and promote these together with a quantum deformation of their Poisson algebra to operators in a Lie algebra. This is not a fundamentally different approach from the first; yet it does add the possibility of choosing an enlarged set of phase space functions that are not independent.

We have tried to find a reparametrization of the boosts. The restricted pairs of boost triples are shown in figure 4.8. As a way to parametrize only the triples satisfying the triangle inequality, we can first extract a common scale factor s from a boost triple. Then a triangle remains to be parametrized. We can exploit its symmetry by choosing three coordinate axes as in figure 5.1. Now a point in this triangle can be written as $\vec{x} = \sum_{i=1}^3 c_i \vec{e}_i$, but there is a redundancy in this description, which can be lifted by imposing the constraint $C = 1 - \sum_{i=1}^3 c_i \approx 0$. We also have to restrict the range of the coefficients: $c_i \in \mathbb{R}_+$ suffices, because it implies $c_i \in [0, 1]$ together with the constraint. Furthermore, a consistent quantization exists on $L^2(\mathbb{R}_+)$, see [9].

This approach does not solve all problems. The new variables are a linear combination of the boosts, so the Poisson brackets will still be of the same form.

³A symplectic transformation is a transformation on a space, which has a symplectic form defined on it. That is in our case: a phase space with a Poisson bracket, where the symplectic transformation by definition preserves the symplectic form (thus the Poisson bracket).

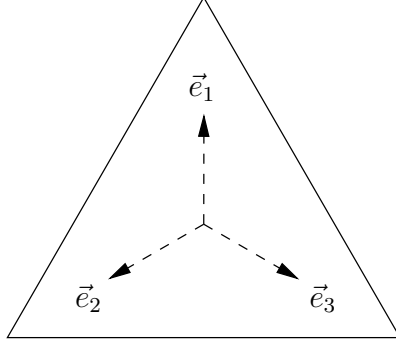


Figure 5.1: Coordinates used to parametrize a triangle.

Since the new coordinates c_i have a restricted domain, the same problem will arise from the Stone–Von Neumann theorem. Next to that, this way of parametrizing the boosts introduces new variables c_i per vertex, while each boost is connected to two vertices. Thus, one would have to introduce constraints of the form $c_i^1 \approx c_j^2$ for each boost, where 1 and 2 label the two vertices a boost is connected to.

Some remarks can be made about an approach in the way mentioned above. We have seen that quantization using variables that obey the canonical commutation relations gives problems with the eigenvalue spectrum. There is also the problem that the constraints (and Hamiltonian) are very complex non-polynomial expressions in terms of the boosts. This will probably give rise to severe operator ordering ambiguities when we try to implement these constraints at the quantum level, if suitable quantum representations can be found at all.

To circumvent these problems, we can look for a set of phase space functions that do not obey the canonical commutation relations and in terms of which the constraints are functionally simpler. As an ansatz we propose the functions $l_i, \sigma_j = \sinh(\eta_j)$ and $\gamma_j = \cosh(\eta_j)$. These have the advantage that the linearity of the constraints in the lengths is preserved and the expressions obviously become simpler in terms of σ_j, γ_j . The angles are given in terms of inverse (co)sines of rational functions of the σ_j, γ_j and thus not polynomial yet. These functions obey the Poisson algebra

$$\begin{aligned} \{l_i, \sigma_j\} &= \frac{1}{2} \delta_{ij} \gamma_j, \\ \{l_i, \gamma_j\} &= \frac{1}{2} \delta_{ij} \sigma_j, \\ \{\sigma_i, \gamma_j\} &= 0, \end{aligned} \tag{5.8}$$

which are not the canonical commutation relations anymore. We now want to find a representation of this algebra such that l and γ have positive spectrum. We have not worked out whether choosing $\hat{l}_i, \hat{\sigma}_j, \hat{\gamma}_j$ as quantum operators yields a consistent quantization scheme though.

A different approach would be to only use variables associated with a set of fundamental loops of the spatial manifold Σ_g . With each such loop we can associate a Poincaré transformation, determined by 6 parameters and there are $2g-1$ independent loops. If we could rewrite the polygon model in terms of these variables, there would only be 3 constraints left. The $6(2g-1)$ variables are 6 more than the $12(g-1)$ dimensions of the physical phase space; 3 of these are constraints and the other 3 are gauge freedoms associated to these constraints.

5.4 Conclusions

The original question whether space is quantized or time is discretized seems to depend on the way one quantizes the theory. This fact is well known, see e.g. [17] or [3, chap. 13].

To draw conclusions about discreteness, one must first have a consistent quantization scheme. In this chapter we saw, that the obvious choice of canonical commutation relations has some serious problems which cannot be overcome easily. Most notably the problem that the spectrum of the basic quantum operators conflicts with the classical length and boost constraints. Therefore it seems that one should not draw conclusions about the spectra of length and time, without first showing that a consistent quantization scheme can (at least theoretically) be found.

6 The constraint algebra

In this chapter, we will do some explicit calculations to determine some properties of the algebra of Poisson brackets of the constraints. Next, we try to interpret these constraints and the transformations they generate.

The algebra of constraints expresses how a constraint transforms under an infinitesimal gauge transformation with respect to another constraint. In the case of first class constraints, the result should be equal to zero on the constraint surface (a so-called ‘weak equality’), because a classical solution must satisfy these constraints and a gauge transformation preserves the solution and thus the constraint too.

The calculation of the constraint algebra is interesting from different perspectives. It allows us to check that these weak equalities hold, which is a consistency check for the polygon model. Furthermore, if one wants to quantize the model and implement the constraints in the quantum theory, then this Poisson algebra should have an analogue in terms of operator commutators in the quantum theory. If they are not equal, this could give rise to quantum anomalies [3, p. 279].

The constraints do not form a true Poisson algebra, because the right-hand sides of the Poisson brackets turn out to be non-linear expressions in terms of the original constraints and thus the linear span of the constraints does not form a closed space under the Poisson brackets. A true Poisson algebra is a vector space X with multiplication and a bi-linear and anti-symmetric Poisson bracket

$$\{ \cdot, \cdot \} : X \times X \mapsto X, \quad (6.1)$$

satisfying the Jacobi identity. Thus when we choose a basis e_i of X , we can write

$$\{ e_i, e_j \} = f_{ij}^k e_k, \quad (6.2)$$

where the f_{ij}^k are the so-called structure constants.

Our algebra of constraints is not of this form, but can (in principle) be rewritten in a form where the structure constants f_{ij}^k are replaced by structure functions $f_{ij}^k(l, \eta)$ on phase space. For a proof, see [3, p. 8 and appendix 1.A]: the Poisson brackets turn out to vanish on the constraint surface and can thus be written as linear combinations of the constraints, with coefficients given by structure functions. These structure functions are not explicitly given however and might be very complicated.

6.1 Useful formulas

Before starting the calculation, we summarize the constraints and some useful relations, which will be used to calculate the Poisson brackets. For each polygon we have two constraints: the angular constraint C_θ and the complex (closure) constraint C_z . They are (4.7):

$$C_\theta^A = \sum_{j=1}^N (\pi - \alpha_j) - 2\pi,$$

$$C_z^A = \sum_{j=1}^N l_j \exp(i\theta_j) \quad \text{where} \quad \theta_j = \sum_{i=1}^j \pi - \alpha_i.$$

The label $A = 1 \dots P$ labels the different polygons. The complex constraint takes values in \mathbb{C} , so it is actually two real constraints. Instead of working with the real and imaginary part, C_z^A and \bar{C}_z^A will be used to calculate all independent Poisson brackets.

Next we have the vertex relations (4.4), from which the following identities can be derived:

$$\frac{\partial \alpha_a}{\partial \eta_a} = -2 \frac{\sigma_a}{s_a \sigma_b \sigma_c}, \quad (6.3)$$

$$\frac{\partial \alpha_a}{\partial \eta_b} = -2 \frac{c_c \sigma_a}{s_a \sigma_b \sigma_c} = 2 \frac{\sigma_b \gamma_c + c_a \sigma_c \gamma_b}{s_a \sigma_b \sigma_c}, \quad (6.4)$$

where the indices a, b, c label the three different edges and angles at a vertex according to figure 2.1. Note that these results differ by a factor 2 from those in [18] (appearing from chain-rule differentiation of the 2η arguments).

The rightmost expression of (6.4) contains only quantities that can be expressed in terms of boosts and angles of a single polygon at that vertex. This can be used to derive another useful relation between neighboring edges and angles along a polygon:

$$\begin{aligned} & e^{\pm i\alpha_{k+1}} \left(\frac{\partial \alpha_{k+1}}{\partial \eta_{k+1}} \mp 2i \frac{\gamma_{k+1}}{\sigma_{k+1}} \right) \\ &= 2 (c_{k+1} \pm i s_{k+1}) \frac{\sigma_{k+1} \gamma_k + c_{k+1} \sigma_k \gamma_{k+1} \mp i s_{k+1} \sigma_k \gamma_{k+1}}{s_{k+1} \sigma_k \sigma_{k+1}} \\ &= 2 \frac{c_{k+1} \gamma_k \sigma_{k+1} + \sigma_k \gamma_{k+1}}{s_{k+1} \sigma_k \sigma_{k+1}} \pm 2i \frac{\gamma_k}{\sigma_k} \\ &= \frac{\partial \alpha_{k+1}}{\partial \eta_k} \pm 2i \frac{\gamma_k}{\sigma_k} \end{aligned} \quad (6.5)$$

The relation $e^{i(\pi-\alpha_j)} = -e^{-i\alpha_j}$ is used throughout the calculations; together with the formula above, we can use it to simplify expressions a lot, as we will see.

As most of the work needed to calculate the different Poisson brackets is very much alike, we will first derive two general expressions, which will be used in further calculations. Both expressions are of the form

$$\sum_{k=1}^N e^{\pm i\Phi_k} \frac{\partial \theta_j}{\partial \nu_k}, \quad (6.6)$$

where we have two polygons and differentiate angles of the first (indices j) with respect to boosts of the second (indices k). θ_j, Φ_k denote the angles of edges as in (4.6). This expression is calculated both for the two polygons being equal and different. In these calculations we make some assumptions (6.11), which can be found in the next section on page 40.

First for j, k indexing the same polygon, we have

$$\begin{aligned} & \sum_{k=1}^N e^{\pm i\theta_k} \frac{\partial \theta_j}{\partial \eta_k} \\ &= - \sum_{k=1}^N e^{\pm i\theta_k} \sum_{l=1}^j \frac{\partial \alpha_l}{\partial \eta_k} \\ &= - \sum_{l=1}^j e^{\pm i\theta_{l-1}} \left(e^{\pm i\theta_N \delta_{l,1}} \frac{\partial \alpha_l}{\partial \eta_{l-1}} + e^{\pm i(\pi-\alpha_l)} \frac{\partial \alpha_l}{\partial \eta_l} \right) \end{aligned}$$

using the fact that angles only depend on neighboring boosts. Notice the extra term $e^{\pm i\theta_N \delta_{l,1}}$: it is present because of the jump in complex angle factor, where the indices are taken cyclic modulo N (but not sums, as noted in (2.5) on page 7). This extra factor is 1 on the constraint surface, but non-trivial away from the constraint surface. Now we plug in the identity $0 = 2i(\frac{\gamma_l}{\sigma_l} - \frac{\gamma_l}{\sigma_l})$ and shift the index of one of the terms to obtain

$$\begin{aligned} &= - \sum_{l=1}^j e^{\pm i\theta_{l-1}} \left(e^{\pm i\theta_N \delta_{l,1}} \left[\frac{\partial \alpha_l}{\partial \eta_{l-1}} \mp 2i \frac{\gamma_{l-1}}{\sigma_{l-1}} \right] + e^{\pm i(\pi-\alpha_l)} \left[\frac{\partial \alpha_l}{\partial \eta_l} \pm 2i \frac{\gamma_l}{\sigma_l} \right] \right) \\ &\quad \pm 2i \left(e^{\pm i\theta_j} \frac{\gamma_j}{\sigma_j} - e^{\pm i\theta_N} \frac{\gamma_N}{\sigma_N} \right) \\ &= \pm 2i \left(e^{\pm i\theta_j} \frac{\gamma_j}{\sigma_j} - e^{\pm i\theta_N} \frac{\gamma_N}{\sigma_N} \right) + (1 - e^{\pm i\theta_N}) \left(\frac{\partial \alpha_1}{\partial \eta_N} \mp 2i \frac{\gamma_N}{\sigma_N} \right) \\ &= \pm 2i \left(e^{\pm i\theta_j} \frac{\gamma_j}{\sigma_j} - \frac{\gamma_N}{\sigma_N} \right) + (1 - e^{\pm i\theta_N}) \frac{\partial \alpha_1}{\partial \eta_N}. \end{aligned} \quad (6.7)$$

In the second last step, we used relation (6.5) to let all terms in the summation cancel against each other, except for the boundary terms.

When the j, k index different polygons, we get (again under the assumptions (6.11)) only a contribution from the common edge denoted by j_c, k_c . This reduces the number of terms in the summation:

$$\begin{aligned}
& \sum_{k=1}^N e^{\pm i \Phi_k} \frac{\partial \theta_j}{\partial \nu_k} \\
&= \sum_{k \in \{k_c-1, k_c, k_c+1\}} e^{\pm i \Phi_k} \times - \sum_{l=1}^j \frac{\partial \alpha_l}{\partial \nu_k} \\
&= -e^{\pm i \Phi_{k_c}} \sum_{k \in \{-1, 0, 1\}} \left(-e^{\pm i(\beta_{k_c} - \Phi_M \delta_{k_c, 1})} \delta_{k, -1} + \delta_{k, 0} - e^{\mp i(\beta_{k_c+1} - \Phi_M \delta_{k_c, M})} \delta_{k, 1} \right) \\
&\quad \times \left(\frac{\partial \alpha_{j_c}}{\partial \nu_{k_c+k}} \delta_{j_c \in [1, j]} + \frac{\partial \alpha_{j_c+1}}{\partial \nu_{k_c+k}} \delta_{j_c+1 \in [1, j]} \right) \\
&= -e^{\pm i \Phi_{k_c}} \left[\left(\frac{\partial \alpha_{j_c}}{\partial \nu_{k_c}} - e^{\mp i(\beta_{k_c+1} + \Phi_M \delta_{k_c, M})} \frac{\partial \alpha_{j_c}}{\partial \nu_{k_c+1}} \right) \delta_{j_c \in [1, j]} \right. \\
&\quad \left. + \left(\frac{\partial \alpha_{j_c+1}}{\partial \nu_{k_c}} - e^{\pm i(\beta_{k_c} + \Phi_M \delta_{k_c, 1})} \frac{\partial \alpha_{j_c+1}}{\partial \nu_{k_c-1}} \right) \delta_{j_c+1 \in [1, j]} \right] \\
&= 2 e^{\pm i \Phi_{k_c}} \left[\left(\frac{c_{k_c+1} \sigma_{k_c+1}}{s_{j_c} \sigma_{j_c-1} \sigma_{j_c}} - e^{\mp i \Phi_M \delta_{k_c, M}} (c_{k_c+1} \mp i s_{k_c+1}) \frac{\sigma_{k_c+1}}{s_{j_c} \sigma_{j_c-1} \sigma_{j_c}} \right) \delta_{j_c \in [1, j]} \right. \\
&\quad \left. + \left(\frac{c_{k_c} \sigma_{k_c-1}}{s_{j_c+1} \sigma_{j_c} \sigma_{j_c+1}} - e^{\pm i \Phi_M \delta_{k_c, 1}} (c_{k_c} \pm i s_{k_c}) \frac{\sigma_{k_c-1}}{s_{j_c+1} \sigma_{j_c} \sigma_{j_c+1}} \right) \delta_{j_c+1 \in [1, j]} \right]
\end{aligned}$$

where the term $e^{\pm i \Phi_M} = 1$ on the constraint surface and we split off $(1 - e^{\pm i \Phi_M}) \dots$, giving

$$\begin{aligned}
&= 2 e^{\pm i \Phi_{k_c}} \left[\pm i \frac{s_{k_c+1} \sigma_{k_c+1}}{s_{j_c} \sigma_{j_c-1} \sigma_{j_c}} \delta_{j_c \in [1, j]} \mp i \frac{s_{k_c} \sigma_{k_c-1}}{s_{j_c+1} \sigma_{j_c} \sigma_{j_c+1}} \delta_{j_c+1 \in [1, j]} \right. \\
&\quad + (1 - e^{\mp i \Phi_M \delta_{k_c, M}}) e^{\mp i \beta_{k_c+1}} \frac{\sigma_{k_c+1}}{s_{j_c} \sigma_{j_c-1} \sigma_{j_c}} \delta_{j_c \in [1, j]} \\
&\quad \left. + (1 - e^{\pm i \Phi_M \delta_{k_c, 1}}) e^{\pm i \beta_{k_c}} \frac{\sigma_{k_c-1}}{s_{j_c+1} \sigma_{j_c} \sigma_{j_c+1}} \delta_{j_c+1 \in [1, j]} \right] \\
&= \pm 2 i e^{\pm i \Phi_{k_c}} \frac{1}{\sigma_{j_c}} (\delta_{j_c \in [1, j]} - \delta_{j_c+1 \in [1, j]}) \\
&\quad - 2 (1 - e^{\pm i \Phi_M}) \frac{1}{s_{\beta_1} \sigma_{\nu_{k_c}}} \left[\delta_{j_c+1 \in [1, j]} \delta_{k_c, 1} + e^{\mp i \beta_1} \delta_{j_c \in [1, j]} \delta_{k_c, M} \right]. \tag{6.8}
\end{aligned}$$

Most of the above calculation is a straightforward expansion of the definitions. However one must keep good track of the indices and cyclic boundary conditions, which make the result non-trivial: if $j = N$ and $k \notin \{1, M\}$ then the result reduces to zero identically. Thus we see here already that the result depends on the choice of labelling of the polygons from the $\delta_{k_c,1}$ and $\delta_{k_c,M}$ terms.

6.2 Calculation of the algebra

We want to calculate the complete Poisson algebra. All different, independent Poisson brackets between the constraints are given by

$$\{C_\theta^A, C_\theta^B\}, \{C_\theta^A, C_z^B\}, \{C_z^A, C_z^B\}, \{C_z^A, \bar{C}_z^B\}, \quad (6.9)$$

where A, B independently run over all polygons. All other combinations can be obtained by using anti-symmetry of the Poisson brackets or by complex conjugation, for example:

$$\{C_\theta^A, \bar{C}_z^B\} = \overline{\{C_\theta^A, C_z^B\}}.$$

To start with, there are some constraints which are trivially equal to zero. First of all, each constraint commutes with itself (when also the polygon labels are identical: $A = B$). Secondly

$$\{C_\theta^A, C_\theta^B\} = 0 \quad (6.10)$$

because there is no dependence on the edge lengths in either constraint.

Next we will calculate the Poisson brackets between all remaining constraints under some non-generic assumptions. Similar calculations were made previously in [18]. Here, we will perform the calculation more explicitly and establish several corrections to the results obtained in [18]. These results we will then use as a starting point for calculating the general form of the algebra, thus lifting the assumptions (6.11).

The assumptions are as follows:

$$\textit{no single polygon has two edges that have to be identified and} \quad (6.11a)$$

$$\textit{no two different polygons have more than one edge in common.} \quad (6.11b)$$

These assumptions are a theoretical, but also practical restriction, as they do not cover the ‘one polygon tessellations’ (OPT’s, as in [13]). There every edge of the polygon has to be identified with another edge of the same, single polygon. OPT’s are the simplest tessellations possible and therefore a practical set of tessellations

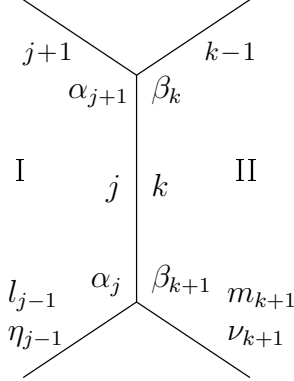


Figure 6.1: Label scheme for the calculation of the constraint algebra

to parametrize phase space with. If we want to explicitly use these OPT's as a starting point for a quantum theory, we therefore need the full Poisson structure without the assumptions.

We will calculate the explicit expressions for the general Poisson structure without these assumptions and show that the constraints do also close in that case. This will be treated in section 6.3 and a summary of all results will be presented in section 6.4.

When we calculate brackets between two different polygons (labeled I and II), the result will be zero unless these polygons have an edge in common. This is because the constraints only depend on variables locally at the border of the polygon. Hence with our assumptions we only have to look at cases where two different polygons have exactly one edge in common.

In the calculations that follow, we will parametrize the two polygons as in figure 6.1. We label lengths, boosts and angles of polygon I with l, η, α respectively and j indexes these. For polygon II we use m, ν, β with indices k . The indices of the edges of polygon I and II that join each other will be denoted by j_c and k_c respectively. Labelling will always be counterclockwise oriented, see also chapter 2.

We start by calculating the Poisson bracket of the angular constraint with the complex constraint of the same polygon. As there is no dependence on the lengths in the C_θ , we only have to differentiate it with respect to the boosts and thus C_z only with respect to the lengths. This yields

$$\begin{aligned} & \{ C_\theta^I, C_z^I \} \\ &= \left\{ \theta_N, \sum_{k=1}^N l_k e^{i\theta_k} \right\} \end{aligned}$$

$$\begin{aligned}
&= -\frac{1}{2} \sum_{k=1}^N e^{i\theta_k} \frac{\partial \theta_N}{\partial \eta_k} && \text{using definition (2.6)} \\
&= -\frac{1}{2} \left(\frac{\partial \alpha_1}{\partial \eta_N} - 2i \frac{\gamma_N}{\sigma_N} \right) (1 - e^{i\theta_N}) && \text{using (6.7)} \\
&= - \left(\frac{\sigma_N \gamma_1 + c_1 \sigma_1 \gamma_N}{s_1 \sigma_1 \sigma_N} - i \frac{\gamma_N}{\sigma_N} \right) (1 - e^{i\theta_N}) \\
&= e^{i\theta_1} \left(\frac{\sigma_1 \gamma_N + c_1 \sigma_N \gamma_1}{s_1 \sigma_1 \sigma_N} + i \frac{\gamma_1}{\sigma_1} \right) (1 - e^{i\theta_N}) \approx 0. \tag{6.12}
\end{aligned}$$

In the last step we used equation (6.5) to rewrite the result to the same form as in [18]. It coincides with the latter expression up to a factor $2e^{i(\pi-\alpha_1)}$; the exponential is due to a different definition of the complex constraint and the factor 2 probably due to a calculation error, as noted below (6.4).

When we take the complex constraint together with its complex conjugate, we get terms from both differentiating the first with respect to the boosts and the second with respect to the lengths and vice versa:

$$\begin{aligned}
&\{ C_z^I, \bar{C}_z^I \} \\
&= \left\{ \sum_{j=1}^N l_j e^{i\theta_j}, \sum_{k=1}^N l_k e^{-i\theta_k} \right\} \\
&= \frac{1}{2} \sum_{j,k=1}^N \left(l_k e^{i\theta_j} e^{-i\theta_k} \times -i \frac{\partial \theta_k}{\partial \eta_j} - l_j e^{i\theta_j} e^{-i\theta_k} \times i \frac{\partial \theta_j}{\partial \eta_k} \right) \\
&= -\frac{i}{2} \sum_{k=1}^N l_k e^{-i\theta_k} \left[+2i \left(e^{i\theta_k} \frac{\gamma_k}{\sigma_k} - \frac{\gamma_N}{\sigma_N} \right) + (1 - e^{i\theta_N}) \frac{\partial \alpha_1}{\partial \eta_N} \right] \\
&\quad -\frac{i}{2} \sum_{j=1}^N l_j e^{i\theta_j} \left[-2i \left(e^{-i\theta_j} \frac{\gamma_j}{\sigma_j} - \frac{\gamma_N}{\sigma_N} \right) + (1 - e^{-i\theta_N}) \frac{\partial \alpha_1}{\partial \eta_N} \right] \quad \text{using (6.7)} \\
&= \frac{\gamma_N}{\sigma_N} (C_z^I - \bar{C}_z^I) - \frac{i}{2} \frac{\partial \alpha_1}{\partial \eta_N} \left[C_z^I (1 - e^{-i\theta_N}) + \bar{C}_z^I (1 - e^{i\theta_N}) \right] \\
&= 2i \frac{\gamma_N}{\sigma_N} \Im(C_z^I) - i \frac{\partial \alpha_1}{\partial \eta_N} \Re(C_z^I (1 - e^{-i\theta_N})) \approx 0. \tag{6.13}
\end{aligned}$$

This result is somewhat different than that in [18]: in the first term we have a relative minus sign instead of plus and the second “boundary” term is added; it arises due to the cyclicity of the edge and angle indices, but one has to be careful with the interpretation of sums of angles as noted in (2.5).

Notice that the correctness of the minus sign is easily checked by complex conjugating the complete Poisson brackets, because it should satisfy

$$\overline{\{C_z, \bar{C}_z\}} = \{\bar{C}_z, C_z\} = -\{C_z, \bar{C}_z\}. \quad (6.14)$$

We can check that the second term does also obey this condition.

Next we have the Poisson brackets between two different polygons. Using equation (6.8) we get

$$\begin{aligned} & \{C_\theta^I, C_z^{II}\} \\ &= \left\{ \theta_N, \sum_{k=1}^M m_k e^{i\Phi_k} \right\} \\ &= -\frac{1}{2} \sum_{k=1}^M e^{i\Phi_k} \frac{\partial \theta_N}{\partial \nu_k} \\ &= -i e^{i\Phi_{k_c}} \frac{1}{\sigma_{j_c}} (\delta_{j_c \in [1, N]} - \delta_{j_c+1 \in [1, N]}) \\ &\quad + (1 - e^{i\Phi_M}) \frac{1}{s_{\beta_1} \sigma_{\nu_{k_c}}} (\delta_{j_c+1 \in [1, j]} \delta_{k_c, 1} + e^{-i\beta_1} \delta_{j_c \in [1, j]} \delta_{k_c, M}) \\ &= (1 - e^{i\Phi_M}) \frac{1}{s_{\beta_1} \sigma_{\nu_{k_c}}} (\delta_{k_c, 1} + e^{-i\beta_1} \delta_{k_c, M}) \approx 0 \end{aligned} \quad (6.15)$$

by straightforward calculation, where we have to remember that the indices are cyclic and thus trivially $\delta_{j_c \in [1, N]} - \delta_{j_c+1 \in [1, N]} = 1 - 1 = 0$. Comparing again with [18], we have found an additional boundary term arising from cyclicity of the indices along the polygon.

The calculation of Poisson brackets between two complex constraints gives

$$\begin{aligned}
& \{ C_z^I, C_z^{\text{II}} \} \\
&= \left\{ \sum_{j=1}^N l_j e^{i\theta_j}, \sum_{k=1}^M m_k e^{i\Phi_k} \right\} \\
&= \frac{i}{2} \sum_{j,k} \left(m_k e^{i\theta_j} e^{i\Phi_k} \frac{\partial \Phi_k}{\partial \eta_j} - l_j e^{i\theta_j} e^{i\Phi_k} \frac{\partial \theta_j}{\partial \nu_k} \right) \\
&= \sum_{k=1}^M m_k e^{i\Phi_k} \left[-\frac{e^{i\theta_{j_c}}}{\sigma_{k_c}} (\delta_{k_c \in [1,k]} - \delta_{k_c+1 \in [1,k]}) \right. \\
&\quad \left. - \frac{i}{s_{\alpha_1} \sigma_{\eta_{j_c}}} (1 - e^{i\theta_N}) (\delta_{k_c+1 \in [1,k]} \delta_{j_c,1} + e^{-i\alpha_1} \delta_{k_c \in [1,k]} \delta_{j_c,N}) \right] \\
&\quad - \{l, \eta, \theta, j\} \leftrightarrow \{m, \nu, \Phi, k\} \quad \text{inserting (6.8)} \\
&= -\frac{e^{i\Phi_{k_c}}}{\sigma_{k_c}} C_z^I \delta_{j_c,N} + \frac{e^{i\theta_{j_c}}}{\sigma_{j_c}} C_z^{\text{II}} \delta_{k_c,M} \\
&\quad - \frac{i}{s_{\alpha_1} \sigma_{\eta_{j_c}}} (1 - e^{i\theta_N}) \left[Z_{k_c+1}^{\text{II}} \delta_{j_c,1} + e^{-i\alpha_1} Z_{k_c}^{\text{II}} \delta_{j_c,N} \right] \\
&\quad + \frac{i}{s_{\beta_1} \sigma_{\nu_{k_c}}} (1 - e^{i\Phi_M}) \left[Z_{j_c+1}^I \delta_{k_c,1} + e^{-i\beta_1} Z_{j_c}^I \delta_{k_c,M} \right] \approx 0, \tag{6.16}
\end{aligned}$$

where we have defined

$$Z_k^A = \sum_{j=k}^N l_j e^{i\theta_j} \tag{6.17}$$

as the partial complex constraint of polygon A from edge k . Also, we used the relations

$$\delta_{j_c \in [1,j]} - \delta_{j_c+1 \in [1,j]} = \delta_{j,j_c} - \delta_{j_c,N} \quad \text{and} \quad \delta_{j_c \in [1,j]} = \delta_{j \in [j_c,N]}. \tag{6.18}$$

Completely analogously, we find for a complex and complex-conjugate constraint

$$\begin{aligned}
& \{ C_z^I, \bar{C}_z^{\text{II}} \} \\
&= +\frac{e^{-i\Phi_{k_c}}}{\sigma_{k_c}} C_z^I \delta_{j_c,N} - \frac{e^{i\theta_{j_c}}}{\sigma_{j_c}} \bar{C}_z^{\text{II}} \delta_{k_c,M} \\
&\quad + \frac{i}{s_{\alpha_1} \sigma_{\eta_{j_c}}} (1 - e^{i\theta_N}) \left[\bar{Z}_{k_c+1}^{\text{II}} \delta_{j_c,1} + e^{-i\alpha_1} \bar{Z}_{k_c}^{\text{II}} \delta_{j_c,N} \right] \\
&\quad + \frac{i}{s_{\beta_1} \sigma_{\nu_{k_c}}} (1 - e^{-i\Phi_M}) \left[Z_{j_c+1}^I \delta_{k_c,1} + e^{i\beta_1} Z_{j_c}^I \delta_{k_c,M} \right] \approx 0. \tag{6.19}
\end{aligned}$$

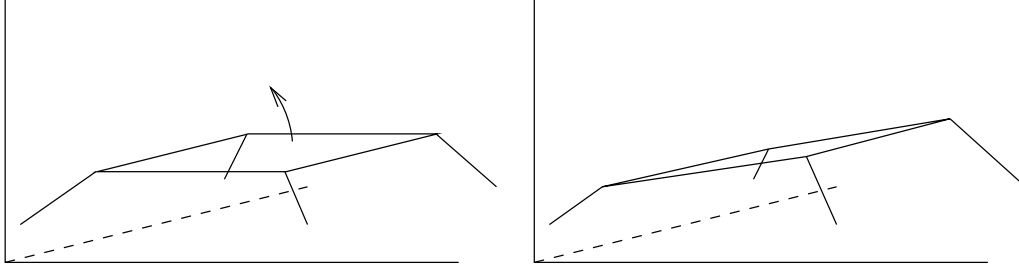


Figure 6.2: Rotation of the plane of a polygon and its action on edge lengths and extrinsic curvature surrounding the polygon.

Both of these Poisson brackets yield expressions that vanish on the constraint surface, but do not identically vanish on the whole phase space, unlike the results in [18]: when one of the indices j_c, k_c is equal to the first or last of its polygon, the result is non-zero.

As already pointed out in [6], the Hamiltonian flow generated by the complex constraints should (on shell) be related to Lorentz transformations of the coordinate frames of the polygons. This is a residual gauge freedom that is left after fixing the constraints \mathcal{H}^i in (3.8). With this interpretation, one would not expect the Poisson brackets between these constraints to vanish identically (as is the result in [18]): the complex constraint should be related to the constraints \mathcal{H}^i and their corresponding gauge freedom to the Lorentz transformations of the local frame of the polygon.

Suppose now that the complex constraint in polygon I does not close by an amount d in the y -direction ($C_z^I = i d \neq 0$) and we generate a Lorentz transformation in polygon I. This Lorentz transformation can be seen as a “space-time rotation” of the plane of polygon I as in figure 6.2: the (infinitesimal) boost of the Lorentz transformation corresponds to an angle that the plane of polygon I is rotated by. This will affect the lengths and boosts of all edges along that polygon and also the lengths of edges connected to those. We now consider the effect of this transformation on a neighboring polygon II. We suppose that they have an edge in common, which has indices j_c, k_c in polygons I and II respectively, where we choose $j_c = N, k_c = M$. The implicit assumption is made that the closure deficit C_z^I is located between edges $j = N$ and $j = 1$. Now the position of vertex 1 (which is located between edges $j = N$ and $j = 1$) depends on whether we view it as the first or last point of the constraint C_z^I , see figure 6.4, where we have implicit complex coordinates $z = x + i y$ and the origin is placed at vertex 1 viewed as starting point of the complex constraint.

This will give rise to a different change of the intersection line under this Lorentz transformation and thus a change in C_z^II . Figure 6.3 shows the geometrical picture in the (y, t) -plane. The lines are the planes of polygons I and II and

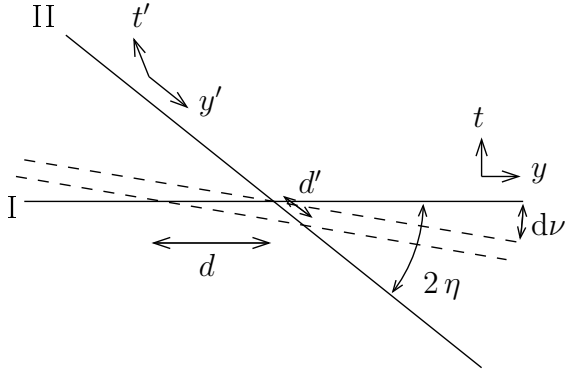


Figure 6.3: Action of a Lorentz transformation on a complex constraint. (y, t) and (y', t') denote the coordinates within polygons I and II respectively.

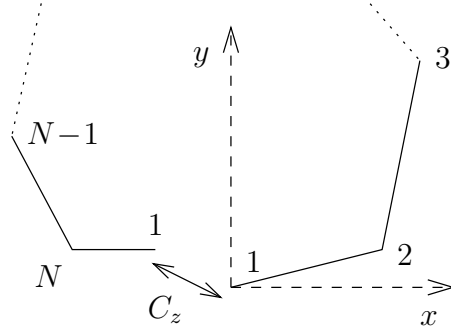


Figure 6.4: Polygon with non-closing complex constraint: vertex 1 shows up on both sides of the deficit $C_z \neq 0$.

their intersection point is the common edge. Now vertex 1 shows up as this intersection point, but also at a distance d apart.

The action of an infinitesimal Lorentz transformation of polygon I by an amount $d\nu$ is shown as the dashed lines. The upper one is rotated around the origin of polygon I (which is vertex 1) and the lower one around vertex 1 as viewed after going around polygon I, after which it is shifted by a distance d . These generate different new intersection points between polygons I and II. We can now calculate the distance between those intersection points explicitly, which yields

$$d' = \frac{d}{\sinh(2\eta)} d\nu. \quad (6.20)$$

This matches the result

$$\{C_z^{\text{II}}, C_z^{\text{I}}\} = \frac{e^{i\Phi_{k_c}}}{\sigma_{k_c}} C_z^{\text{I}} \delta_{j_c, N} = \frac{id}{\sigma}, \quad (6.21)$$

where we have inserted that all constraints close, except $C_z^{\text{I}} = id$ and thus all other terms from (6.16) vanish and $\Phi_M = 2\pi$.

Thus this geometrical viewpoint seems to indicate that indeed the Poisson bracket $\{C_z^{\text{I}}, C_z^{\text{II}}\}$ is not identically zero outside the constraint surface, if we interpret the complex constraints as generators of Lorentz transformations.

6.3 Generalizations

We can generalize the assumptions (6.11) made in the previous section to the arbitrary case, which will recover the explicit full Poisson structure. We will take two different approaches: the first one is to consider the Poisson brackets of the constraints with the Hamiltonian, using the Hamiltonian flow in (4.8). The Hamiltonian is the sum of the angular constraints, so for an OPT we have $H = C_\theta$. This will then give us the Poisson bracket $\{C_\theta, C_z\}$ in the case of an OPT without any assumptions made. The second approach will be to lift the assumptions in a general setting. The results of these approaches are then shown to match in the case of an OPT.

6.3.1 The case of an OPT

To calculate the Poisson bracket $\{H, C_z\}$, we first need a formula relating the growth of edges along a polygon. This formula and its derivation is analogous to (6.8). However we note that in the definition of the σ, γ in (6.22), the factor 2 is missing with respect to our original definition (2.4), so $\sigma_i = \sinh(\eta_i), \gamma_i = \cosh(\eta_i)$. We have

$$\begin{aligned}
& e^{\pm i\alpha_{k+1}} \left(l_{k+1,1} \pm i \frac{\sigma_{k+1}}{\gamma_{k+1}} \right) \\
&= -(c_{k+1} \pm i s_{k+1}) \frac{\sigma_k \gamma_{k+1} + c_{k+1} \sigma_{k+1} \gamma_k \mp i s_{k+1} \sigma_{k+1} \gamma_k}{s_{k+1} \gamma_k \gamma_{k+1}} \\
&= -\frac{\sigma_{k+1} \gamma_k + c_{k+1} \sigma_k \gamma_{k+1}}{s_{k+1} \gamma_k \gamma_{k+1}} \mp i \frac{\sigma_k}{\gamma_k} \\
&= l_{k,2} \mp i \frac{\sigma_k}{\gamma_k}. \tag{6.22}
\end{aligned}$$

We can use the previous relation to rewrite $\{C_z, H\}$ (the time evolution of the complex constraint) in the same way as we did with (6.12):

$$\begin{aligned}
& \{C_z, H\} \\
&= \left\{ \sum_{j=1}^N l_j e^{i\theta_j}, H \right\} \\
&= \sum_{j=1}^N e^{i\theta_j} \dot{l}_j \\
&= \sum_{j=1}^N e^{i\theta_j} \left(\dot{l}_{j,1} - i \frac{\sigma_j}{\gamma_j} + \dot{l}_{j,2} + i \frac{\sigma_j}{\gamma_j} \right)
\end{aligned}$$

$$\begin{aligned}
&= e^{i\theta_1} \left(l_{1,1} - i \frac{\sigma_1}{\gamma_1} \right) (1 - e^{i\theta_N}) && \text{using (6.22)} \\
&= \left(l_{N,2} + i \frac{\sigma_N}{\gamma_N} \right) (e^{i\theta_N} - 1) \\
&= \left(-\frac{v_N c_1 + v_1}{s_1} + i v_N \right) (e^{i\theta_N} - 1) \approx 0 && (6.23)
\end{aligned}$$

Here we recognize the left part of the final expression as minus the velocity of vertex 1 in the coordinate-frame of the polygon (in complex notation, as was used for the formulation of the complex constraint). The factor $e^{i\theta_N} - 1$ precisely gives the difference of viewing this point as the first or the last when going around the polygon. Thus this intuitively matches the expected result of the time evolution of the closure constraint.

6.3.2 The case of a general tessellation

We now want to generalize the calculated Poisson brackets between two polygons to the arbitrary case without assumptions (6.11).

The underlying idea is as follows: we can split the Poisson bracket expression into parts (see (6.25) for a precise specification), taking account for each common edge separately. For this, we first have to show that there are some restrictions to the ways two polygons can have multiple edges in common, such that we can make such a splitting. For this to work, different common edges should not interfere with each other in the calculation of the Poisson brackets.

To show that the “condition” above is fulfilled, let us consider two polygons as in figure 6.5, which have at least an edge in common for edge indices j_c, k_c . The polygons X, Y and Z can be copies of polygons I or II and as such can give rise to multiple common edges.

The only non-vanishing terms in the Poisson brackets appear from the differentiation of one term in a complex (conjugate) constraint (say polygon II) to the edge length and then the other constraint (polygon I) differentiated with respect to the corresponding boost. This means differentiation of an angle of polygon I, as the angles are the only quantities in the constraints that depend on boosts.

If two common edges cannot appear in such a way that their ‘split’ Poisson brackets would both contain a specific angle term of polygon I being differentiated to a boost of the same edge of polygon II, we can replace the Poisson brackets by two separate Poisson brackets where we treat the common edges one at a time. Note that here an ‘edge’ is a boundary element of a polygon, so each pair (l_i, η_i) is assigned to two edges, when the edges are viewed as boundaries of polygons.

Thus the “condition” above can be stated in a more precise way as follows:

each edge from polygon II has at most one way in which it is connected to each angle of polygon I (and the converse, which follows from (6.24) interchanging polygons I and II).

The proof of this statement hinges on the fact that the graph of the tessellation has trivalent vertices. We will first give an insightful proof followed by a more detailed proof.

The statement can be seen to hold in the following way. If an angle would be connected twice to an edge, then this edge has its endpoints on one vertex. Because of trivalency of the vertices, both ends of that edge must be neighboring at that vertex and thus the edge encloses a polygon in itself. This is clearly a contradiction.

For the detailed proof, we start off with the case of an angle of polygon I and an edge of polygon II. Proving (6.24) boils down to a tedious but straightforward treatment of all possible scenario's. With some symmetry arguments, we can however reduce this a bit. Suppose that an angle of polygon I is connected twice to an edge of polygon II. It must be an angle at one side of a common edge. Because of symmetry we can take angle α as shown in figure 6.5 without loss of generality.

Now edge k_c cannot be connected to α more than once, because it is already joined with edge j_c and thus cannot be joined with $j_c - 1$ and it cannot be equal to edge $k_c + 1$. Also edge $k_c + 1$ cannot be connected more than once, because if it would be connected to $j_c - 1$ (as b), then k_c would be connected to $k_c + 1$ (as a). Finally, edges a and b obviously cannot be equal, so condition (6.24) is fulfilled for angles of polygon I.

To apply the idea as outlined above to the generalization of the Poisson brackets, we first have to explicitly define what we mean by a splitting of a Poisson bracket

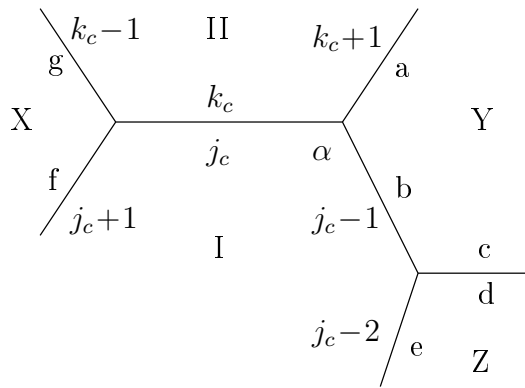


Figure 6.5: Multiple common edges between two polygons.

into separate parts for each common edge. Let us denote the pairs of common edges of polygon A and B by $(j_c, k_c)_{c=1..n_c}$. We now introduce the notation

$$\{ C^A, C^B \}_0 \quad \text{and} \quad \{ C^A, C^B \}_c. \quad (6.25)$$

The left expression shall denote the Poisson brackets of two constraints, where no edges are identified. This expression will thus only be non-zero when $A = B$ and then yields the ‘internal terms’. The right expression shall denote the Poisson brackets of these constraints, where no internal contributions are counted (so we treat $A \neq B$) and only the edge pair (j_c, k_c) is treated as common; the others are treated as not being common. Thus by their definitions, these expressions are equal to the corresponding expression calculated in section 6.2 under the assumptions (6.11): $\{ C^A, C^B \}_0$ for the case $A = B$ and $\{ C^A, C^B \}_c$ for the case $A \neq B$. We will generalize the Poisson brackets already calculated to arbitrary conditions, by proving that one can split the general Poisson brackets as

$$\{ C^A, C^B \} = \{ C^A, C^B \}_0 + \sum_{c=1}^{n_c} \{ C^A, C^B \}_c. \quad (6.26)$$

Given two polygons I and II, we denote their pairs of common edges by $(j_c, k_c)_{c=1..n_c}$ and first investigate the Poisson brackets $\{ \theta_j^I, C_z^{\text{II}} \}$:

$$\begin{aligned} & \sum_{c=1}^{n_c} \{ \theta_j^I, C_z^{\text{II}} \}_c \\ &= \sum_{c=1}^{n_c} \left[\{ -\alpha_{j_c} \delta_{j_c \in [1, j]}, m_{k_c-1} e^{i\Phi_{k_c-1}} + m_{k_c} e^{i\Phi_{k_c}} \} + \right. \\ & \quad \left. \{ -\alpha_{j_c+1} \delta_{j_c+1 \in [1, j]}, m_{k_c} e^{i\Phi_{k_c}} + m_{k_c+1} e^{i\Phi_{k_c+1}} \} \right] \\ &= \sum_{j'=1}^j \{ -\alpha_{j'}, C_z^{\text{II}} \} \\ &= \{ \theta_j^I, C_z^{\text{II}} \} \end{aligned} \quad (6.27)$$

Working backward from the desired result, we first only write down those terms that will contribute for each common edge. In the next step, we use the fact that each combination of angle α of polygon I and edge m of polygon II does show up not more than once in the full Poisson bracket, as stated in (6.24). It also does show up exactly once, as it is part of a single common edge bracket. All remaining terms in $\{ \theta_j^I, C_z^{\text{II}} \}$ are zero now, because we have exactly taken into account all terms contributing to all common edge Poisson brackets and there are no internal contributions, because we considered two different polygons.

In the case that both constraints are from the same polygon, we can essentially repeat the argument, except that we have to add the terms that arise from the internal contributions:

$$\begin{aligned}
& \{ \theta_j^I, C_z^I \}_0 + \sum_{c=1}^{n_c} \{ \theta_j^I, C_z^I \}_c \\
&= \sum_{k=1}^N \{ -\alpha_k \delta_{k \in [1,j]} - \alpha_{k+1} \delta_{k+1 \in [1,j]}, l_k e^{i\theta_k} \} + \\
& \quad \sum_{c=1}^{n_c} \left[\{ -\alpha_{j_c} \delta_{j_c \in [1,j]}, l_{k_c-1} e^{i\theta_{k_c-1}} + l_{k_c} e^{i\theta_{k_c}} \} + \right. \\
& \quad \left. \{ -\alpha_{j_c+1} \delta_{j_c+1 \in [1,j]}, l_{k_c} e^{i\theta_{k_c}} + l_{k_c+1} e^{i\theta_{k_c+1}} \} \right] \\
&= \sum_{j'=1}^j \{ -\alpha_{j'}, C_z^{\text{II}} \} \\
&= \{ \theta_j^I, C_z^{\text{II}} \}. \tag{6.28}
\end{aligned}$$

The extra terms do not change the argument, because also with these added, condition (6.24) still holds and all terms that we started with are exactly those that will be present in the full Poisson bracket.

Now that we have shown in (6.27) and (6.28) that a split can be made for the brackets $\{ \theta_j^A, C_z^B \}$ for all A, B , we can easily extend the result to all possible Poisson brackets. The application of (6.27) to $\{ C_\theta^I, C_z^{\text{II}} \}$ is trivial by plugging in $j = N$ and yields

$$\begin{aligned}
& \{ C_\theta^I, C_z^{\text{II}} \} \\
&= \sum_{c=1}^{n_c} \{ C_\theta^I, C_z^{\text{II}} \}_c \quad \text{using (6.27)} \\
&= \sum_{c=1}^{n_c} (1 - e^{i\Phi_M}) \frac{1}{s_{\beta_1} \sigma_{\nu_{k_c}}} (\delta_{k_c,1} + e^{-i\beta_1} \delta_{k_c,M}) \approx 0. \tag{6.29}
\end{aligned}$$

We see that the sum over all joined pairs of edges (j_c, k_c) reduces to only contributions from the pairs where $k_c = 1$ or $k_c = N$.

In the same way, we can generalize $\{C_\theta^I, C_z^I\}$ using (6.28), which gives

$$\begin{aligned}
& \{C_\theta^I, C_z^I\} \\
&= \{C_\theta^I, C_z^I\}_0 + \sum_{c=1}^{n_c} \{C_\theta^I, C_z^I\}_c \\
&= - \left(\frac{\sigma_N \gamma_1 + c_1 \sigma_1 \gamma_N}{s_1 \sigma_1 \sigma_N} - i \frac{\gamma_N}{\sigma_N} \right) (1 - e^{i\theta_N}) \\
&\quad + \sum_{c=1}^{n_c} (1 - e^{i\Phi_M}) \frac{1}{s_{\beta_1} \sigma_{\nu_{k_c}}} (\delta_{k_c,1} + e^{-i\beta_1} \delta_{k_c,M}) \approx 0. \tag{6.30}
\end{aligned}$$

To generalize the Poisson brackets of two complex (conjugate) constraints to the case of multiple common edges, we first rewrite one complex constraint to a sum of θ_j by the chain rule for differentiation and obtain

$$\begin{aligned}
& \{C_z^I, C_z^{\Pi}\} \\
&= \left\{ \sum_{j=1}^N l_j e^{i\theta_j}, \sum_{k=1}^M m_k e^{i\Phi_k} \right\} \\
&= i \sum_{j=1}^N l_j e^{i\theta_j} \{\theta_j, C_z^{\Pi}\} - i \sum_{k=1}^M m_k e^{i\Phi_k} \{\Phi_k, C_z^I\} \\
&= i \sum_{j=1}^N l_j e^{i\theta_j} \sum_{c=1}^{n_c} \{\theta_j, C_z^{\Pi}\}_c - i \sum_{k=1}^M m_k e^{i\Phi_k} \sum_{c=1}^{n_c} \{\Phi_k, C_z^I\} \\
&= \sum_{c=1}^{n_c} \{C_z^I, C_z^{\Pi}\}_c \tag{6.31}
\end{aligned}$$

The Poisson brackets where one of the constraints is a complex conjugate and when both constraints are from the same polygon, are all derived in an analogous way. For the explicit expression one must insert the already calculated brackets with assumptions. See (6.32b) and (6.32c) for the complete expressions.

6.3.3 Comparing for consistency

Now we can do a consistency check with the results we have found. The Hamiltonian can be written as the sum of all angular constraints. The Poisson brackets of this sum of all angular constraints with one complex constraint should thus match expression (6.23). Indeed we find that they do match:

$$\begin{aligned}
& \{ H, C_z^B \} \\
&= \sum_A \{ C_\theta^A, C_z^B \} \\
&= \{ C_\theta^B, C_z^B \} + \sum_{A \neq B} \{ C_\theta^A, C_z^B \} \\
&= - \left(\frac{\sigma_N \gamma_1 + c_1 \sigma_1 \gamma_N}{s_1 \sigma_1 \sigma_N} - i \frac{\gamma_N}{\sigma_N} \right) (1 - e^{i\Phi_M}) \\
&\quad + \sum_{k=1}^M (1 - e^{i\Phi_M}) \left(\frac{1}{s_1 \sigma_1} \delta_{k,1} + \frac{e^{-i\beta_1}}{s_1 \sigma_M} \delta_{k,M} \right)
\end{aligned}$$

where we sum over all angular constraints, so all separate summations over common edges reduce to one summation over all edges of polygon B. This sum then reduces to the two terms $k = 1$ and $k = M$, which leaves us with

$$\begin{aligned}
&= (1 - e^{i\Phi_M}) \left[-\frac{\sigma_M \gamma_1 + c_1 \sigma_1 \gamma_M}{s_1 \sigma_1 \sigma_M} + i \frac{\gamma_M}{\sigma_M} + \frac{1}{s_1 \sigma_1} + \frac{e^{-i\beta_1}}{s_1 \sigma_M} \right] \\
&= (1 - e^{i\Phi_M}) \left[-\frac{1}{s_1} \left(\frac{\gamma_1 - 1}{\sigma_1} + c_1 \frac{\gamma_M - 1}{\sigma_M} \right) + i \frac{\gamma_M - 1}{\sigma_M} \right] \\
&= \left(-\frac{v_1 + c_1 v_N}{s_1} + i v_N \right) (1 - e^{i\theta_N}) \quad \text{using } \frac{\gamma - 1}{\sigma} = v \\
&= - \{ C_z^B, H \} \quad \text{inserting (6.23).}
\end{aligned}$$

Note that we replaced θ 's by Φ 's when inserting (6.30) and vice versa when rewriting the result back to (6.23), but these are the same as both constraints describe the same polygon.

6.4 Summary

The results of this chapter are summarized below. The same conventions have been made and the sums are again over all pairs of common edges between polygons A and B . In the case that A and B are equal, each pair will thus show up twice: if the pair $(j_c, k_c) = (x, y)$ exists, then also $(j_c, k_c) = (y, x)$.

$$\begin{aligned} \{ C_\theta^A, C_z^B \} = & - \left(\frac{\sigma_N \gamma_1 + c_1 \sigma_1 \gamma_N}{s_1 \sigma_1 \sigma_N} - i \frac{\gamma_N}{\sigma_N} \right) (1 - e^{i\theta_N}) \delta_{A,B} \\ & + \sum_{c=1}^{n_c} \left((1 - e^{i\Phi_M}) \frac{1}{s_{\beta_1} \sigma_{\nu_{k_c}}} (\delta_{k_c,1} + e^{-i\beta_1} \delta_{k_c,M}) \right) \end{aligned} \quad (6.32a)$$

$$\begin{aligned} \{ C_z^A, C_z^B \} = & \sum_{c=1}^{n_c} \left(- \frac{e^{i\Phi_{k_c}}}{\sigma_{k_c}} C_z^A \delta_{j_c,N} + \frac{e^{i\theta_{j_c}}}{\sigma_{j_c}} C_z^B \delta_{k_c,M} \right. \\ & - \frac{i}{s_{\alpha_1} \sigma_{\eta_{j_c}}} (1 - e^{i\theta_N}) \left[Z_{k_c+1}^B \delta_{j_c,1} + e^{-i\alpha_1} Z_{k_c}^B \delta_{j_c,N} \right] \\ & \left. + \frac{i}{s_{\beta_1} \sigma_{\nu_{k_c}}} (1 - e^{i\Phi_M}) \left[Z_{j_c+1}^A \delta_{k_c,1} + e^{-i\beta_1} Z_{j_c}^A \delta_{k_c,M} \right] \right) \end{aligned} \quad (6.32b)$$

$$\begin{aligned} \{ C_z^A, \bar{C}_z^B \} = & \left(\frac{\gamma_N}{\sigma_N} (C_z^A - \bar{C}_z^A) - \frac{i}{2} \frac{\partial \alpha_1}{\partial \eta_N} \left[C_z^A (1 - e^{-i\theta_N}) + \bar{C}_z^A (1 - e^{i\theta_N}) \right] \right) \delta_{A,B} \\ & + \sum_{c=1}^{n_c} \left(+ \frac{e^{-i\Phi_{k_c}}}{\sigma_{k_c}} C_z^A \delta_{j_c,N} - \frac{e^{i\theta_{j_c}}}{\sigma_{j_c}} \bar{C}_z^B \delta_{k_c,M} \right. \\ & + \frac{i}{s_{\alpha_1} \sigma_{\eta_{j_c}}} (1 - e^{i\theta_N}) \left[\bar{Z}_{k_c+1}^B \delta_{j_c,1} + e^{-i\alpha_1} \bar{Z}_{k_c}^B \delta_{j_c,N} \right] \\ & \left. + \frac{i}{s_{\beta_1} \sigma_{\nu_{k_c}}} (1 - e^{-i\Phi_M}) \left[Z_{j_c+1}^A \delta_{k_c,1} + e^{i\beta_1} Z_{j_c}^A \delta_{k_c,M} \right] \right) \end{aligned} \quad (6.32c)$$

6.5 Interpretation

We would like to interpret the Poisson bracket relations we have found. The angular and complex constraints are first class constraints and should correspond to some residual constraints and gauge freedom left after the (partial) fixing of the constraints $\mathcal{H}, \mathcal{H}^i$ in (3.7) and (3.8).

Intuitively, the residual constraint left from the Hamiltonian density \mathcal{H} is the sum of deficit angles at the vertices. Superficially, this seems to match the angular constraints, but in these the sum of deficit angle at a vertex is distributed among the angular constraints of polygons that join at that vertex.

The complex constraints should be related to the residual gauge freedom of Lorentz transformations of each polygon frame. With the help of the dual graph formulation of appendix A, we can try to see whether this intuitive idea matches the explicit complex constraint definition. In the dual graph, a Lorentz transformation of a polygon frame $f \in F$ amounts to shifting the corresponding vertex $\tilde{v} \in \tilde{V}$ in the dual graph by the action of the Lorentz transformation L when we choose \tilde{v} to be at the origin $(1, 0, 0)$.

The boosts η_i of edges along the polygon are encoded by half the arc lengths of the geodesics emanating from \tilde{v} . Thus if we make an infinitesimal Lorentz transformation, the change in boosts will be half the “length” of the Lorentz transformation projected on the direction of the outgoing edge (as seen in the dual graph). This means that a Lorentz transformation of boost $d\nu$ in the x direction in the polygon frame should affect the boosts η_i as follows:

$$d\eta_i = \cos(\phi) d\nu, \quad (6.33)$$

with ϕ the angle that edge i makes with the x axis in the dual graph. This angle is $\phi = \theta_i + \frac{\pi}{2}$, because the direction of the boost is perpendicular to the direction of the edge in the normal graph.

We can compare this to the gauge transformation generated by the complex constraint. The action of that gauge transformation is given by the Hamiltonian flow; the Poisson brackets of a quantity with the constraint gives the action that the corresponding gauge transformation has on that quantity. For the boosts we find

$$d\eta_i = \{ \eta_i, C_z \} = -\frac{1}{2} \frac{\partial C_z}{\partial l_i} = -\frac{1}{2} e^{i\theta_i} = -\frac{1}{2} (\cos(\theta_i) + i \sin(\theta_i)). \quad (6.34)$$

Comparing this with (6.33), we see that the imaginary part of C_z generates Lorentz transformations in the x direction and the real part in the negative y direction, at least for the boost variables.

Unfortunately, the action on the length variables is much more complicated. To compare the action on the lengths of the complex constraint with the action of a

Lorentz transformation, we can consider the action of a Lorentz transformation of the polygon frame geometrically and check whether that matches $\{l_i, C_z\}$. In the geometrical picture of the tessellation graph, one expects that an (infinitesimal) Lorentz transformation acts on the variables as a “rotation in space-time” of the polygon plane, see figure 6.2. This changes the intersection lines with its neighboring polygons, from which the action of the Lorentz transformation on the lengths can be deduced. The explicit formulation of this action is also quite complicated and we have not investigated whether this geometrical picture matches the Poisson brackets.

7 Conclusions

We have looked at the polygon model as a way to describe $2+1$ -dimensional gravity. This model makes use of the local flatness of $2+1$ D space-time in a remarkably efficient way: the polygon model can be formulated as a finite dimensional system with a completely explicit description of its evolution in terms of growth of edge lengths and polygons undergoing transitions at a discrete set of times. This makes the model very useful for exploring features of gravity already in the classical context, e.g. by simulation.

In well known other descriptions of $2+1$ -dimensional gravity, the system is defined more implicitly. For example in the ADM formulation with York time, one must solve the conformal factor of the metric from a elliptic partial differential equation. This has no known explicit solution for genus $g > 1$ [14]. Witten's approach seems to use the frozen time picture, where the dynamics cannot be recovered from the system [15, 19]. These problems are not present in the polygon model formulation.

There are however also some drawbacks of the formulation of the polygon model. The polygons that together form a spatial slice, are of finite size and internally flat by construction. In this construction we have solved the field equations of the gauge constraints. The finite dimensional system which is left, is (by definition) non-local and still has constraints. This yields difficulties.

The problems of this non-locality are most clear in the Poisson bracket structure of the constraints. The constraints for each polygon are already non-local expressions and the Poisson brackets of constraints between different polygons are complicated expressions, which do not vanish off shell. Even stronger, they do not form a proper Poisson algebra, because the brackets are not linear in the constraints.

We have shown though, that the complete Poisson bracket structure can be calculated explicitly and does vanish on shell. This was expected, as the constraints should be a residue of the field constraints in the unreduced canonical formulation, which are first class.

The features of the polygon model that allowed an explicit formulation in the classical theory become problematic when we turn to the question of quantization. First of all, a full description of a state depends partially on a discrete graph

structure, which changes under transitions. This cannot easily be encoded in a quantum formulation. Furthermore, there are inequality constraints which are coupled in a very non-local way. This is due to the fact that the Hamiltonian is a highly non-trivial function of the basic variables, which is only defined when those inequalities are satisfied. Because of these inequalities, we cannot lift the simple Poisson bracket structure between those coupled variables to a quantum theory, as that would violate these triangle inequalities.

We have shown that several ways of attacking the problem of finding a consistent quantization run into one or more of the difficulties above. Thus the question of whether the polygon model obtains a discrete time and/or space spectrum after quantization seems to be premature. It not only depends on whether one first quantizes and then implements the constraints or vice versa, but more fundamentally on whether a satisfactory quantum theory can be formulated in either approach. If we first quantize, we face a complicated Poisson structure which has to be implemented in the quantum theory. If we first solve the constraints, we face the problem of finding an explicit global solution to those.

Both approaches, although meeting some major obstacles, do not seem completely hopeless. The dual graph formulation (as in appendix A) gives a nice abstract interpretation of the polygon model, which might be useful to reduce the constraints in the classical theory in terms of holonomy-loop variables. This dual graph formulation depends on the absence of particles however. On the quantum theory side, one might consider other variables than the canonical ones. This leaves the question of whether this polygon model can be quantized to a difficult but open one.

A The dual graph

In this appendix we will present the dual graph of a tessellation in the polygon model. For this we will first introduce the concept of a dual graph in its general setting and also introduce hyperbolic space. It turns out that we can assign a meaning to the dual graph of a tessellation, such that it becomes a graph embedded in a hyperbolic space: a surface with constant negative curvature.

A.1 The dual of a planar graph

The concept of a dual graph is a very general one within graph theory and has applications in a wide variety of fields. It does not add new information to the graph, but allows one to see some features more quickly by using a different representation of the same graph data.

To introduce the dual graph, we start with a graph $G = (V, E)$, where V is the set of its vertices and E the set of edges. Each edge is normally represented as a pair of vertices: the ones that it connects. If we now embed our graph in the plane, the dual of that graph is defined by associating a vertex to each region of the plane and connect two vertices with an edge when their regions in the original graph had an edge as a common boundary. One must however notice two things: firstly, not every graph can be embedded in the plane without intersecting edges, so this definition does not yield a dual graph for each graph (V, E) . Secondly, a graph can have different possible embeddings in the plane, resulting in different dual graphs; see figures A.1 and A.2 for an example.

This non-uniqueness of the dual graph can be lifted if we add faces to the graph information. We now write $G = (V, E, F)$ with F a set of faces and each edge also containing information about the pair of faces it connects. We want this graph with added faces to uniquely describe a graph on some genus g surface. This means that we have an orientation¹ in the graph from the underlying manifold

¹The orientation can only be defined locally in the case of a generic surface. However we only consider orientable surfaces, which allows us to extend this local orientation to a global one.

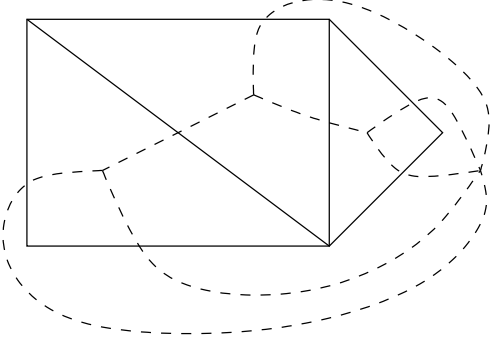


Figure A.1: A graph embedded in the plane with its dual graph (dotted lines).

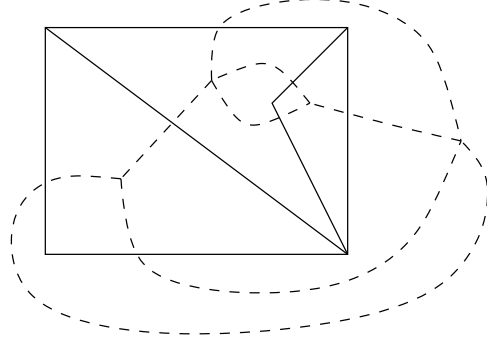


Figure A.2: The same graph embedded differently with a different dual (dotted lines).

and that at each vertex and face, we have an ordered list of the edges that “connect” to that vertex or face.

With this added structure, we can assign a unique dual graph \tilde{G} to each graph $G = (V, E, F)$ by mapping vertices of G to faces of \tilde{G} and faces of G to vertices of \tilde{G} . The edges are mapped to themselves with the pairs of vertices and faces they connect interchanged. So we have $\tilde{G} = (\tilde{V}, \tilde{E}, \tilde{F}) = (F, E, V)$.

Given this definition we can observe some facts. These only depend on the graph structure, because at this point we have not yet added any additional information to the graph, like edge lengths.

When we take the dual of the dual graph, we get back the original graph:

$$\tilde{\tilde{G}} = G. \quad (\text{A.1})$$

From the geometrical picture of viewing the graph embedded in a surface, we see that a graph G and its dual \tilde{G} represent graphs on surfaces of the same homotopy class. When we look at the Euler characteristic χ of the graph, we find the same result, because we have

$$\chi = 2 - 2g = \#V - \#E + \#F, \quad (\text{A.2})$$

where g is the genus of the (orientable) surface.

A.2 Hyperbolic space

Hyperbolic space is a Riemannian manifold. Its most common definition (and most practical here) is as follows. For $n \geq 2$, start with an $(n+1)$ -dimensional Minkowski space, thus \mathbb{R}^{n+1} with the metric² $\eta^{\mu\nu} = \text{diag}(-1, 1, \dots)$. Now n -dimensional hyperbolic space is defined as

$$\mathbb{H}^n = \{x \in \mathbb{R}^{n+1} \mid \eta(x, x) = -1, x_0 > 0\} \quad (\text{A.3})$$

with the metric induced from the underlying Minkowski space.

The space thus constructed is a true Riemannian manifold: the original metric was a pseudo-Riemannian metric, but its restriction to \mathbb{H}^n is positive definite. Furthermore \mathbb{H}^n is a space with constant negative (sectional) curvature -1 : at any point p and any 2-dimensional plane in the tangent space of p , the scalar curvature is -1 .

We will be concerned specifically with the case $n = 2$: the hyperbolic plane. The hyperbolic plane has some other well-known representations, besides the definition (A.3) given above. One is that of the complex halfplane

$$\{x + iy \in \mathbb{C} \mid y > 0\}, \quad ds^2 = \frac{dx^2 + dy^2}{y^2}, \quad (\text{A.4})$$

and the other is the unit disc

$$\{(x, y) \in \mathbb{R}^2 \mid \|(x, y)\| < 1\}, \quad ds^2 = \frac{dx^2 + dy^2}{1 - \|(x, y)\|^2}. \quad (\text{A.5})$$

These two models are known as the Poincaré plane and disc respectively.

Hyperbolic space is a maximally symmetric Riemannian manifold. That means that its isometry group is as large as can possibly be for a Riemannian manifold, namely, of dimension $\frac{1}{2}n(n+1)$. We will further investigate this symmetry from the viewpoint of our original definition (A.3). The symmetry group is the identity component $SO^+(n, 1)$ of the full Lorentz group $O(n, 1)$. The group $SO^+(n, 1)$ consists of the time- and space-orientation preserving Lorentz transformations on the Minkowski space \mathbb{R}^{n+1} and thus preserves the metric η and the sign of x_0 .

This group $SO^+(n, 1)$ can now be seen to have a group action on \mathbb{H}^n : an element $L \in SO^+(n, 1)$ defines a map $L : \mathbb{R}^{n+1} \mapsto \mathbb{R}^{n+1}$ that can be restricted to a map $L : \mathbb{H}^n \mapsto \mathbb{H}^n$, because $SO^+(n, 1)$ precisely preserves the quantities that define

²This can be interpreted as the metric on Minkowski space itself and the differential metric on the tangent space as Minkowski space is a vector space and thus isomorphic to its tangent space.

\mathbb{H}^n . This map L then also naturally defines the map $DL : T\mathbb{H}^n \mapsto T\mathbb{H}^n$ on the tangent bundle.

The elements $L \in SO^+(n, 1)$ exactly correspond to all possible isometries of \mathbb{H}^n . This is because the group $SO^+(n, 1)$ has precisely $\frac{1}{2}n(n+1)$ degrees of freedom: n degrees correspond to translations of the hyperbolic plane and $\frac{1}{2}n(n-1)$ correspond to rotations around a fixed origin.

Looking in detail at how $SO^+(n, 1)$ acts on \mathbb{H}^n , we see for $n = 2$ that pure Lorentz boosts $L_{x,y}(\eta)$ perform translations in \mathbb{H}^n by a distance of η in the x, y -direction (locally around the “origin” $(1, 0, 0)$; because of curvature the action is somewhat more complicated away from the origin). The rotations $L_r(\alpha)$ perform a simple rotation around the origin.

A.3 Embedding the dual graph in \mathbb{H}^2

We have first constructed the dual graph of a tessellation. Let us now assign geometrical data to this dual graph.

We will do so by looking at the path that a Lorentz transformation maps out in hyperbolic space when it acts on $(1, 0, 0)$. Each Lorentz transformation L can be decomposed into pure rotations and boosts in the following way:

$$L = L_r(\phi_1) L_x(\eta) L_r(\phi_2). \quad (\text{A.6})$$

This can be interpreted (in reverse order) as rotating the local frame over an angle ϕ_1 to the direction of the boost, then boost with parameter η and then rotate the boosted frame to the desired orientation over an angle ϕ_2 . The continuous transformation of $(1, 0, 0)$ under the one-parameter subgroup

$$L(t) = L_r(\phi_1) L_x(\eta t) L_r(\phi_2), \quad t \in [0, 1] \quad (\text{A.7})$$

will then be a geodesic in \mathbb{H}^2 ; figure A.3 shows an example of such geodesics.

Now each edge in the dual graph corresponds to a Lorentz³ transformation L of one frame to the other it connects. Actually, we should consider oriented edges, because when we traverse the edge in opposite direction, the Lorentz transformation is L^{-1} . Thus each edge can be viewed as an isometry of \mathbb{H}^2 , which in turn can be viewed as geodesics in \mathbb{H}^2 .

A triangular polygon in the dual graph corresponds to a vertex in the original graph. Thus traversing its three enclosing edges means going around that vertex and the composition of corresponding Lorentz transformations should be the

³We can more generally assign to each edge a Poincaré transformation, by also taking into account the way coordinates are shifted after crossing an edge.

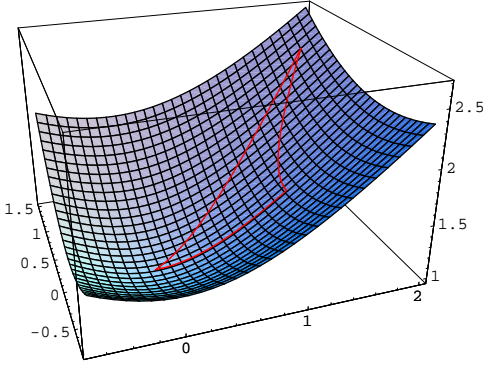


Figure A.3: The hyperbolic surface \mathbb{H}^2 with red lines showing a triangle: the successive action of boosts and rotations, forming a closed holonomy.

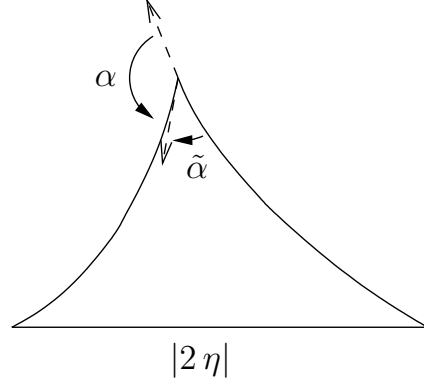


Figure A.4: Angles of a hyperbolic triangle.

identity. This means that, again viewing these edges as geodesics in \mathbb{H}^2 , they form a closed triangle and we can thus naturally associate a graph structure with it, see figure A.3.

We can now try to interpret the geometrical data of this graph embedded in \mathbb{H}^2 : the dual graph lives in a Riemannian manifold, so concepts like lengths and angles are well-defined. Some subtleties will show up however, due to the fact that these geodesics do not contain all information of the Lorentz transformations of the edges. Each Lorentz transformation L is fully characterized by the way it acts as an isometry on \mathbb{H}^2 , but if we only look at its action on a single point, information is lost: the way it acts on other points. This can be retrieved by not only giving the action of L on a single point, but also specifying its action on the tangent space at that point.

When we now draw a triangle in the dual graph like in figure A.4, we find that each edge has geodesic length $|2\eta|$. The outer angles of the triangle are in direct correspondence to the angles α_i at a vertex in the original graph: they describe the rotation that we have to make, when we “walk” along a geodesic and turn to the direction of the next geodesic. The inner angles $\tilde{\alpha}_i$ of the triangle are related to these as

$$\tilde{\alpha}_i = \pi - \alpha_i. \quad (\text{A.8})$$

With this identification, we see that at each vertex in the dual graph, we have a 2π neighborhood as expected:

$$\sum_{i=1}^N \tilde{\alpha}_i = \sum_{i=1}^N \pi - \alpha_i = C_\theta = 2\pi \quad (\text{A.9})$$

by identification of the vertex in the dual graph with a polygon in the original graph and using the angular constraint.

There is also an interpretation for the Hamiltonian (4.9) in the dual graph by considering the area of all faces in the dual graph. We start from the fact that the area of a triangle in hyperbolic space is determined by its inner angles $\tilde{\alpha}_i$ only, as the deficit angle from π :

$$A = \pi - \sum_{i=1}^3 \tilde{\alpha}_i. \quad (\text{A.10})$$

When we now sum the area of all triangles in the dual graph, we obtain

$$A = \sum_{\tilde{f} \in \tilde{F}} \left(\pi - \sum_{i=1}^3 \tilde{\alpha}_i \right) = - \sum_{v \in V} \left(2\pi - \sum_{i=1}^3 \alpha_i \right) = -H. \quad (\text{A.11})$$

The boost parameters 2η cannot be interpreted as simply the geodesic lengths: η can be negative and in the geometric picture of figure A.4 this corresponds to walking the geodesic line in the opposite direction.

If we have a vertex where the signs of the three boosts are not the same (called a ‘mixed vertex’ in [13]), this implies that the interpretation of $\tilde{\alpha}_i = \pi - \alpha_i$ as the inner angles of the triangle becomes problematic.

A way to solve this is to consider again the Lorentz transformations corresponding to each edge. These can be decomposed as in (A.6). In decomposing these we can always choose η positive: if it is negative, we can replace the parameters by $(\phi_1, \eta, \phi_2) \mapsto (\phi_1 \pm \pi, -\eta, \phi_2 \pm \pi)$. In this way we get a graph with all edge lengths positive and the oriented sum of angles at every point a multiple of 2π . If we translate this interpretation back to the original graph, it means that we have reversed the orientation of the edges. This interpretation thus moves the signs from the boosts onto the lengths, which looks similar to the variables x_i, p_j introduced in [6]. This will affect the definition of the Hamiltonian and the equations of motion, but we have not analyzed further the implications.

See also the discussion of this problem of the interpretation of mixed vertices in [12, p. 47].

Acknowledgements

First of all, I would like to thank my supervisor, Prof. Renate Loll for giving me the opportunity to work on this interesting subject. She guided me with my questions to the right places. I would especially like to thank Zoltán Kádár for the numerous discussions I had with him and the detailed proofreading he did.

I also want to thank my fellow students in MG301 for the pleasant atmosphere and the innumerable (work related) discussions. In particular I want to express thanks to Gerben, Jan and Lotte for the years of working together during our studies and Gerben for some helpful discussions and ideas.

Bibliography

- [1] Abhay Ashtekar, Stephen Fairhurst and Joshua L. Willis. *Quantum gravity, shadow states, and quantum mechanics*. Class. Quant. Grav., 20:1031–1062, 2003. gr-qc/0207106.
- [2] S. Carlip. *Quantum gravity in 2+1 dimensions*. Cambridge Univ. Pr., 1998. ISBN 0-521-56408-5, 276 pages.
- [3] M. Henneaux and C. Teitelboim. *Quantization of gauge systems*. Princeton Univ. Pr., 1992. ISBN 0-691-08775-X, 520 pages.
- [4] H. R. Hollmann and R. M. Williams. *Hyperbolic geometry in 't Hooft's approach to (2+1)- dimensional gravity*. Class. Quant. Grav., 16:1503–1518, 1999.
- [5] Gerard 't Hooft. *Causality in (2+1)-dimensional gravity*. Class. Quant. Grav., 9:1335–1348, 1992.
- [6] Gerard 't Hooft. *Canonical quantization of gravitating point particles in (2+1)-dimensions*. Class. Quant. Grav., 10:1653–1664, 1993. gr-qc/9305008.
- [7] Gerard 't Hooft. *Classical N particle cosmology in (2+1)-dimensions*. Class. Quant. Grav., 10(S):S79–S91, 1993.
- [8] Gerard 't Hooft. *The evolution of gravitating point particles in (2+1)-dimensions*. Class. Quant. Grav., 10:1023–1038, 1993.
- [9] C. J. Isham. *Topological and global aspects of quantum theory*. In B. S. DeWitt and R. Stora, editors, *Relativity, groups and topology 2*, pages 1062–1290. Elsevier Science Publishers, 1984.
- [10] C. J. Isham. *Canonical quantum gravity and the problem of time*. 1992. gr-qc/9210011.
- [11] Z. Kadar. *Polygon model from first order gravity*. Class. Quant. Grav., 22:809–824, 2005. gr-qc/0410012.

- [12] Z. Kadar. *The polygon representation of three dimensional gravitation and its global properties*. Ph.D. thesis, Utrecht University, Institute for theoretical physics, 2005. URL <http://igitur-archive.library.uu.nl/dissertations/2005-0429-200024/full.pdf>.
- [13] Z. Kadar and R. Loll. *(2+1) gravity for higher genus in the polygon model*. Class. Quant. Grav., 21:2465–2491, 2004. gr-qc/0312043.
- [14] V. Moncrief. *Reduction of the Einstein equations in (2+1)-dimensions to a Hamiltonian system over Teichmuller space*. J. Math. Phys., 30:2907–2914, 1989.
- [15] V. Moncrief. *How solvable is (2+1)-dimensional Einstein gravity?* J. Math. Phys., 31:2978–2982, 1990.
- [16] C.R. Putnam. *Commutation Properties of Hilbert Space Operators and Related Topics*. Springer Verlag, 1967, 167 pages.
- [17] Henri Waelbroeck and Jose A. Zapata. *2 + 1 covariant lattice theory and 't Hooft's formulation*. Class. Quant. Grav., 13:1761–1768, 1996. gr-qc/9601011.
- [18] M. Welling. *The torus universe in the polygon approach to 2+1- dimensional gravity*. Class. Quant. Grav., 14:929–943, 1997. gr-qc/9606011.
- [19] Edward Witten. *(2+1)-dimensional gravity as an exactly soluble system*. Nucl. Phys., B311:46, 1988.